European Journal of Pharmaceutics and Biopharmaceutics 198 (2024) 114240

Contents lists available at ScienceDirect

European Journal of Pharmaceutics and Biopharmaceutics

journal homepage: www.elsevier.com/locate/ejpb

On the uncertainty of the correlation between nanoparticle avidity and biodistribution

Oliver Zimmer, Achim Goepferich *

Department of Pharmaceutical Technology, University of Regensburg, Regensburg, Bavaria 93053, Germany

ARTICLE INFO

Keywords:
Targeted nanoparticles
Biodistribution
Avidity
Particle-cell membrane interactions

ABSTRACT

The specific delivery of a drug to its site of action also known as targeted drug delivery is a topic in the field of pharmaceutics studied for decades. One approach extensively investigated in this context is the use ligand functionalized nanoparticles. These particles are modified to carry receptor specific ligands, enabling them to accumulate at a desired target site. However, while this concept initially appears straightforward to implement, in-depth research has revealed several challenges hindering target site specific particle accumulation - some of which remain unresolved to this day. One of these challenges consists in the still incomplete understanding of how nanoparticles interact with biological systems. This knowledge gap significantly compromises the predictability of particle distribution in biological systems, which is critical for therapeutic efficacy.

One of the most crucial steps in delivery is the attachment of nanoparticles to cells at the target site. This attachment occurs via the formation of multiple ligand receptor bonds. A process also referred to as multivalent interaction. While multivalency has been described extensively for individual molecules and macromolecules respectively, little is known on the multivalent binding of nanoparticles to cells. Here, we will specifically introduce the concept of avidity as a measure for favorable particle membrane interactions. Also, an overview about nanoparticle and membrane properties affecting avidity will be given. Thereafter, we provide a thorough review on literature investigating the correlation between nanoparticle avidity and success in targeted particle delivery. In particular, we want to analyze the currently uncertain data on the existence and nature of the correlation between particle avidity and biodistribution.

1. Introduction

Targeted drug delivery is an intensively studied topic in pharmaceutics [1]. The concept aims for an exclusive distribution of a drug at its intended site of action. This way, an administered dose can efficiently unfold the drugs therapeutic effect, while no other sites are at risk of potential side-effects. One approach employed to achieve targeted drug delivery is the use of nanoparticles [2–4]. Herein, we focus on ligand functionalized nanoparticles [5]. At the core of this concept, the particle surface is modified to carry ligand molecules [6,7] enabling recognition of target site specific cellular receptors [8] or ectoenzymes [9] via a key-lock mechanism. Once the particle encounters its site of action, multiple ligand receptor bonds are formed, attaching the particle to cell surfaces. Thus, the particle is retained at the target site or even induces active uptake into the cell via endocytosis [10,11]. Drug molecules can be incorporated into such particles to enable cell-specific delivery. Molecule-types incorporated into nanoparticles are small-molecular drugs [12], peptides [13,14], biopharmaceuticals [15,16], and nucleic acids of different nature [17–20]. A targeted delivery is very desirable for many applications especially in the case of highly potent agents, such as anti-cancer drugs, which can cause damage in healthy tissues and organs. Also, highly valuable agents such as biologics or vaccines would benefit greatly from targeted delivery [21].

The optimal method to investigate in vivo nanoparticle deposition is to track the whole-body biodistribution [22–25]. A measure for successful targeted delivery is the percentage of administered dose found in the intended cell-type tissue [26]. In pursuing optimized particle distribution, a number of factors have been identified hindering targeted delivery of nanoparticles. Some of the most studied problems, which are mutually dependent to some extent, are the formation of a protein corona on the particle surface [27–29], interaction with immune cells [30], and undesired particle accumulation in typical off-target organs (e.g., liver and spleen) [31–33]. All these phenomena were shown to decrease particle accumulation at the desired site of action while

* Corresponding author.
E-mail address: achim.goepferich@ur.de (A. Goepferich).

https://doi.org/10.1016/j.ejpb.2024.114240
Received 17 November 2023; Received in revised form 5 February 2024; Accepted 28 February 2024
Available online 2 March 2024

increasing loss of particles due to rapid elimination or unspecific deposition [34–37]. While almost all steps in the journey of a particle have been intensively studied [38], it is somewhat surprising that the particle-cell surface interaction has received little attention in studies on nanoparticle biodistribution. Nanoparticle-membrane interactions are often studied in isolated experiments based on artificial or isolated membranes [39–41] using techniques like surface plasmon resonance (SPR) [42] or microscale thermophoresis (MST) [43,44]. These techniques cannot preserve the natural nano-scale morphology of cell membranes. Therefore, we know very little about how these morphological entities affect particle avidity. Concluding, in contrast to membrane properties, we have a good understanding of how particle properties affect quantitative binding parameters like avidity. However, the relationship between avidity and biodistribution has hardly been studied and therefore remains elusive.

In the first part of this work, we will give a brief introduction to the theoretical background on nanoparticle binding to cell surfaces. As nanoparticles are usually multivalently functionalized, we will discuss the fundamental thermodynamics governing the formation of multivalent ligand receptor complexes. Specifically, we will illustrate the term of avidity as a commonly used quantity to describe multivalent interactions of particles binding to receptor carrying cell surfaces. In simple terms, avidity describes the tendency of a particle functionalized with several individual ligands (i.e., multivalent functionalization) to bind to a surface that carries several receptors. It can be understood as the analog value of multivalent systems to the affinity of the single ligand-receptor interaction. Furthermore, we will shed a light on the impact of membrane properties on particle-membrane interactions. Here, we will specifically discuss the often-neglected role of membrane curvature. Overall, this section is intended to provide the reader with a fundamental understanding about particle and membrane properties dictating avidity of nanoparticle membrane binding. We also intend to discuss dose-dependence of nanoparticle biodistribution as an underresearched topic in the context of targeted nanoparticle delivery, which we believe should receive more attention.

In the second part of this work, we intend to provide an overview about studies investigating the impact of particle binding avidity or ligand density on particle biodistribution. We included studies specifically addressing this matter as well as publications providing relevant insights while pursuing a different research goal. Most interesting studies for our purpose to describe effect of nanoparticle avidity on biodistribution were whole-body biodistribution studies. However, we also included studies investigating the impact of avidity on particle distribution on the tissue or cell level. Based on the concepts introduced in the first section, we will elaborate to what extent avidity correlates with nanoparticle biodistribution. In conclusion, we will determine whether the data available in literature indicate a transferability of the theory of avidity to the case of nanoparticle distribution in a complex biological system. In this context, it must be emphasized that by focusing on the particle-cell interaction, a single step of the complex process of particle biodistribution is considered in isolation. Many other factors that influence the biological identity of a particle and thus its biodistribution have already been described. These include, in particular, the opsonization of particle surfaces, which leads to recognition by the immune system and induces the accumulation of particles, e.g., in the liver and spleen [45].

2. Fundamentals of nanoparticle avidity concept

A fundamental understanding of avidity is helpful to follow the work below. An excellent review on this matter is available in the literature [46]. For this reason, here we will give a short, easily accessible overview. For more detailed insights, the interested reader is referred to the relevant original literature. Also, for readers who are less interested in the theoretical background, we have provided a brief summary of the key points after the following two sections.

To begin, we want to look at some thermodynamic models describing the Gibb's energy of a multivalent binding, since we can learn from these models what influencing variables determine avidity. Earliest works leading to thermodynamic models describing avidity of multivalent interactions were conducted by Jencks et al. [47,48]. To properly appreciate the models derived from this, one must consider the intentions of the respective authors. To this end, an initial model developed by Kitov and Bundle is excellently suited for computational simulation of Gibb's free energy of multivalent interactions ($\Delta G^0_{avidity}$) [49]. However, here the properties underlying and determining the avidity of the interacting structures remain somewhat elusive. Therefore, to gain a better insight into these properties, we will also consider the model developed by Krishnamurthy et al. [50] Here it is unraveled in more detail what is behind the possibly hard to grasp thermodynamic parameters. We will see that Krishnamurthy et al. derived their model on Gibb's free energy of multivalent interactions (here denoted as ΔG^0_N (i)), considering individual receptor-ligand interactions as additive and expanding the model by introducing enthalpy (ΔH) and entropy ($T\Delta S$) terms accounting for phenomena inherent of multivalent interactions. In this way, they derive a model from which we can derive properties of multivalent ligand complexes (e.g., ligand functionalized nanoparticles) can be derived, whose variation could affect particle avidity [50].

The model introduced by Kitov and Bundle is based on a simple expression for microscopic free binding energy Δg^0_i (Eq. (1)) of a single interaction between a multivalent ligand L and a receptor R receptor-ligand complex denoted as rl(i). In clear words, rl(i) in our example of ligand functionalized nanoparticles binding to receptor carrying cell membrane would correspond to a single particle forming i ligand receptor bonds. ΔG^0_{mono} is a rather straightforward parameter as it represents the binding free energy of a monovalent interaction. $\Delta G^0_{interaction}$, however, might appear a bit more elusive. This is a parameter introduced to account for differences in the free energy of the first intermolecular bond and all 'intramolecular' bonds formed subsequently.

$$\Delta g_i^0 = i\Delta G^0_{mono} + \Delta G^0_{interaction} \tag{1}$$

Again, transferred to our example of particle-membrane interactions, ΔG^0_{mono} would be the first ligand-receptor bond formed, while $\Delta G^0_{interaction}$ would describe the difference between the free energy of this initial bond and all other bonds formed subsequently.

The authors rearrange their model introducing the terms $\Delta G^0_{mono} = \Delta G^0_{inter}$ and (i-1) ΔG^0_{intra} = (i-1) ΔG^0_{mono} + $\Delta G^0_{interaction}$ which separates the free energy of the bonds formed after the-initial binding took place. Also, the authors extend the so far microscopic model (i.e., accounting for only a single rl(i) complex = a single particle bound to a membrane) to a macroscopic model (i.e., accounting for a large number of rl(i) complexes = particles) by introducing a degeneracy coefficient Ω_i. This is in simple words the number of microscopically distinguishable rl(i) complexes (i.e., in our example the number of particles in the i-th state) (Fig. 1A). The model ultimately has the following form where R is the gas constant and T is the absolute temperature:

$$\Delta G_i^0 = \Delta G^0_{inter} + (i-1)\Delta G^0_{intra} - RT\ln\Omega_i \tag{2}$$

We learn from this first model of the free energy of multivalent interactions that avidity must not be understood as an 'additive' phenomenon. Instead, for multivalent interactions, the bonds already formed influence the formation of further bonds. This property of multivalent interactions is called cooperativity. As cooperativity is a broad topic on its own, we will leave it here with a brief definition of the term. We consider a simple interaction of a monovalent ligand A and a bivalent receptor BB (Fig. 1C). This system can be described by the law of mass as following.

$$2K_1 = \frac{[A \bullet BB]}{[A][BB]} \text{ and } \frac{1}{2}K_2 = \frac{[A_2 \bullet BB]}{[A][A \bullet BB]} \tag{3 and 4}$$

The interaction is called cooperative if the condition

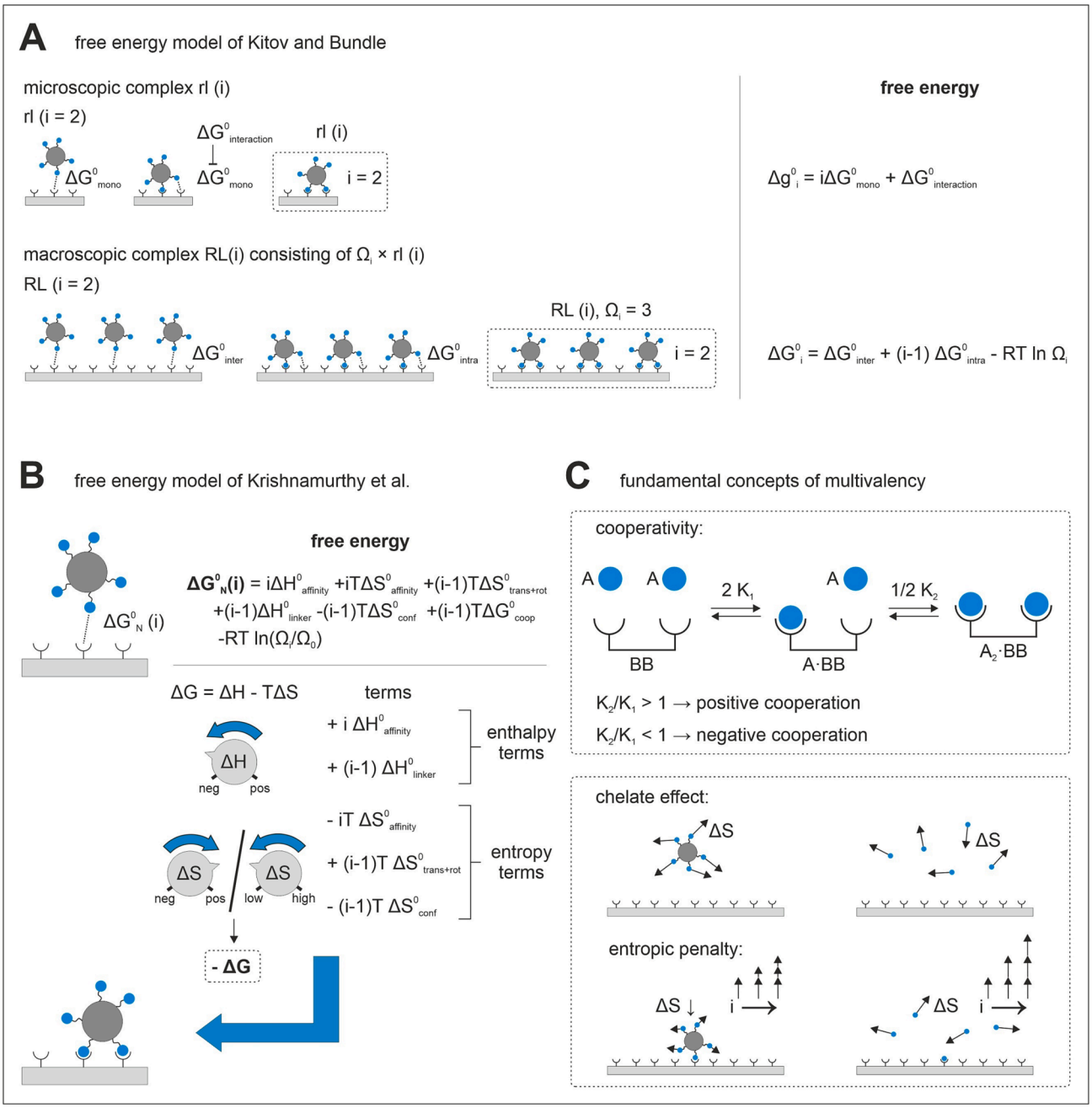

Fig. 1. Fundamental theoretical framework governing the formation of multivalent interactions. (A) The model introduced by Kitov and Bundle initially describes the Gibbs free energy Δg_i^0 of a microscopic receptor ligand complex rl(i). The terms in this model represent the formation of a monovalent intermolecular bond ΔG^0_{mono} while all subsequent intramolecular bonds are described by an interaction term $\Delta G^0_{interaction}$ correcting their free energy for all phenomena inherent to multivalency. This model is expended to (a) apply for the macroscopic scenario of several multivalent ligands L interacting with a multivalent receptor R by introducing a degeneracy factor Ω_i (forming a complex RL(i)), and (b) to consider the initial bond and the subsequent bonds separately (i.e., ΔG^0_{inter} and ΔG^0_{intra}). (B) The model of Krishnamurthy et al. has a slightly different form. Here, the enthalpy and entropy components of relevant properties of the multivalent receptor are summed to obtain the Gibbs free energy $\Delta G^0_N(i)$ of the interaction as a function of the number of formed bonds i. The cooperativity of the interaction is accounted for by a separate free energy term ΔG^0_{coop}. Again, a factor Ω_i/Ω_0 is introduced to obtain a macroscopic model. In this form, the model can be used to derive parameters that affect avidity. (C) Shows knowledge snippets on two key phenomena inherent to most multivalent interactions. Cooperativity describes the effect which the formation of an initial bond to a multivalent receptor exceeds on the formation of subsequent bonds. If the initial bond favors the formation of subsequent bonds a positive cooperativity is present ($K_1 < K_2$). In the opposite case when the initial bond hinders the formation of further bonds, the cooperativity is negative. The chelate effect describes how the attachment of a multivalent ligand via an initial bond reduces the entropy (represented by black arrows) of the not yet receptor-bound ligands tethered to the same backbone. This results in a reduced entropic penalty to be paid upon binding of these ligands compared to the attachment of an equal number of free ligands.

$$\frac{K_2}{K_1} \neq 1 \tag{5}$$

is met. A ratio of the two reaction constants $K_2/K_1 > 1$ indicates a positive cooperativve interaction (i.e., the first bond favors the second bond) while $K_2/K_1 < 1$ indicates a negative cooperative interaction (i.e., the first bond hinders the second bond) [46,51]. However, the model of Kitov and Bundle tells us little about particle properties that can affect

avidity.

Therefore, we next consult the model developed by Krishnamurthy et al. to see if we can draw further insights from it on nanoparticle properties affecting avidity. The model ultimately has the following form:

$$\Delta G_N^0(i) = i\Delta H_{affinity}^0 - iT\Delta S_{affinity}^0 + (i-1)T\Delta S_{trans+rot}^0 + (i-1)\Delta H_{linker}^0$$

$$-(i-1)T\Delta S_{conf}^0 + (i-1)\Delta G_{coop}^0 - RT\ln(\Omega_i/\Omega_0) \quad (6)$$

As this model may seem a bit intimidating at first, let's take a step back. We first consider the general equation of Gibbs energy which is given as follows:

$$\Delta G = \Delta H - T\Delta S \quad (7)$$

If we now take another look at the model, we will see that here enthalpy (ΔH) and entropy (ΔS) amounts are added up to account for different processes. For each term, there is an additional factor that determines whether the corresponding term is to be taken into account for all bonds (i) or for all bonds except the initial bond (i-1). And as we know that a negative free energy ΔG ($\Delta G < 0$) indicates the volatility of a reaction (i.e., in our case, particle binding), we can deduce that to increase the avidity of our particle, the individual terms must be modified to overall achieve, at best, a negative binding enthalpy (-ΔH) and an increase in entropy (+ΔS). However, since we are studying the attachment of a particle to a membrane, an increase in entropy is not to be expected. Therefore, practically a minimum entropy loss is to be aimed for (Fig. 1B). In turn, this gives us indications as to which particle properties determine avidity.

As an example, let us consider the first two terms of the model:

$$\Delta G = \Delta H - T\Delta S$$

$$i\Delta H_{affinity}^0 - iT\Delta S_{affinity}^0 \quad (8)$$

These terms describe the independent formation of all i receptor ligand bonds. This part of the model therefore corresponds to the term ΔG_{mono}^0 in the model of Kitov and Bundle. Note that for instance this expression does not yet account for cooperativity. In the model of Krishnamurthy et al. this is accounted for via a separate free energy term (i-1) ΔG_{coop}^0 which is consequently considered for all bonds except the initial bond, as cooperativity can only occur after the formation of an initial bond. We learn from these first terms of the model that the nature of the ligand and its corresponding receptor will affect the avidity of the particle. An extended collection of free binding energy data has been published in this regard. In this context, there is literature as well as databases available for the selection of ligand-receptor pairs possessing a strongly negative free energy of binding ΔG [52–55].

Let us now go through some more terms to get a clearer understanding about further particle parameters affecting particle avidity. Krishnamurthy et al. stress the importance of the third term:

$$(i-1)T\Delta S_{trans+rot}^0 \quad (9)$$

As this term accounts for another essential concept in multivalent interaction referred to as chelate or multivalency effect. To briefly introduce this concept, on the one hand, we envision a particle to which a certain number of ligands have been functionalized. On the other hand, we consider the same number of unbound ligands. Here, an entropy penalty must be 'paid' for each unbound ligand that attaches to a receptor. Each ligand almost completely loses its translational and rotational mobility upon binding. In the case of the particle, however, after the attachment of the initial ligand the translational and rotational mobility of all other ligands is already significantly reduced as they are all tethered to the same particle. The entropy penalty is therefore reduced for the formation of subsequent bonds (Fig. 1C) [47,48,56]. Since for the first ligand-receptor bond formed, the full entropic penalty has to be paid, this term is considered for all bonds but the initial one (i-1). We can gain a clearer understanding of the influence of this term by considering at the separated fraction of translation entropy (ΔS_{trans}). Finkelstein and Janin derived an estimate for this parameter [57].

$$\Delta S_{trans} \approx 3R\ln\left(\frac{\delta x}{v^{1/3}}\right) \quad (10)$$

Here, δx is the mean amplitude of the bound ligand in the three principal directions (i.e., after attachment), and v is the volume accessible to the ligand in solution (i.e., ahead of attachment). As a simple rule of thumb, we can deduce that the more the ligand is restricted in its freedom of movement due to the binding, the higher the entropic penalty. One way to optimize avidity could be to constrain the mobility of the ligand prior to binding on the particle (e.g., by tightly packing the ligands on the particle surface or rigid linkers). However, ligand mobility has been described as an essential prerequisite for the interaction of particles with membranes [58]. For this reason, we consider it unlikely that the (i-1) $\Delta S_{trans+rot}^0$ term is suitable as a starting point for optimizing avidity.

A promising approach to improve the avidity of a multivalent nanoparticle may lie in the use of cooperative membrane receptors. This would target (i-1) ΔG_{coop}^0 term in the model of Krishnamurthy et al. Beneficial effects would be expected here, however, only in the case of positive cooperativity, in which the formation of the first bond favors that of the second (-ΔG_{coop}^0, Eq. (5)). Concretely, hetero-multivalent functionalized particles could be used, whose first ligand, upon binding to the receptor exposes the high-affinity binding site for the second ligand via a conformational shift. In this way, one could take advantage of receptor allostery. The strategy of allosteric binding cooperativity was already introduced by de Amici et al. with a mainly pharmacological focus [59]. A transfer of this strategy to the targeted delivery of nanoparticles, however, could be promising, considering the introduced models.

Finally, one of the most important factors influencing the avidity of multivalent ligands must be discussed. This is the number of formed bonds i. If we take a negative Gibbs free energy as given (i.e., particle binding will proceed voluntarily), then it alone determines the magnitude of the Gibbs free energy.

To deduce a hypothesis on nanoparticle distribution, let us consider the nanoparticle as a multivalent ligand (L) encountering two cell membrane surfaces (M_1 and M_2) with two different receptor (R) densities (ρ_R^{M1} and ρ_R^{M2}). Under the prerequisite outlined above:

$$L + R \rightarrow LR \text{ has } \Delta G < 0 \quad (11)$$

if

$$\rho_R^{M1} > \rho_R^{M2} \quad (12)$$

than the number of bonds (i) will accordingly vary, resulting in distinct Gibbs free energies for attachment of L to M_1 or M_2:

$$i_{M1} > i_{M2} \rightarrow \Delta G_{L\rightarrow M1} < \Delta G_{L\rightarrow M2} \quad (13)$$

Therefore, making the attachment of L (i.e., multivalently functionalized nanoparticle) to M_1 (i.e., membrane expressing the higher receptor level) favorable over the attachment to M_2. With the equations Eq. (12) and Eq. 13, we formulated the hypothesis to be derived from the introduced model under the assumption of Eq. 11 for the distribution of nanoparticles faced with membranes possessing different receptor densities. Initial supporting evidence for this hypothesis can be found in the work of Martinez-Veracoechea and Frenkel who found in simulations that even the smallest changes in receptor density may have a massive impact on binding behavior [60]. Transferred to the case of nanoparticle biodistribution our hypothesis suggests accumulation in the tissue or organ showing the highest receptor expression. One goal of this work will be to compare the experimental data on biodistribution of ligand-functionalized nanoparticles available in the literature against this hypothesis. For this purpose, we intend to review biodistribution studies

investigating ligand-functionalized nanoparticles, ideally providing quantitative particle binding parameters. Here, dissociation constants (K_D) would be the ideal parameter as K_D relates to the Gibbs free energy by the simple term [61]:

$$\Delta G = RT\ln K_D \tag{14}$$

Finally, we want to discuss limitations of the theoretical framework introduced. For all considerations above, it must be emphasized that the presented models were formulated to describe interactions of oligovalent macromolecules. Whether a simple transferability of these models to the case of a multivalent nanoparticle is given must therefore be critically evaluated. Thus, Krishnamurthy et al. [50] explicitly stress that their model does not account for aggregation of receptors via simultaneous binding of multiple receptors to one oligovalent ligand. The assumption is made that the receptor is strongly diluted. Yet, with respect to ligand-functionalized nanoparticles, the phenomenon of ligand-receptor interaction-induced receptor aggregation has been frequently described [62–64]. A fundamental work on the avidity of multivalent particles was presented by Hong et al. They synthesized 5 poly(amidoamine)-based dendrimers functionalized with controlled amounts of folic acid molecules. Interactions with immobilized folate binding proteins were characterized using surface plasmon resonance (SPR) technique. In this early work, the authors found that avidity expressed as the dissociation constant K_D of dendrimer conjugates decreased with increasing valency, resulting from a linear increase in k_{on} and an exponential decrease in k_{off} [65]. So far, the observations follow the expectations based on the theoretical framework introduced. However, as we will see with the exemplary systems presented below, this observation on the mechanistic origin of avidity seems not to be generally applicable.

3. Impact of membrane curvature on Nanoparticle-Cell interaction

Several papers have systematically investigated the impact of physicochemical nanoparticle properties like size [66–75], surface charge [76–78], and shape [79–82] on biodistribution. However, in this section we would like to shift our focus and shed a light on the counterpart of the particle in multivalent attachment, the cell membrane. Which properties of the membrane affect the interaction? And could a change in the membrane alone alter the avidity of a given particle? We consider these questions highly relevant because in biological systems the composition of cell membranes is constantly changing. Since the properties of membranes are highly sensitive to changes in their composition [83,84], a particle thus continuously encounters membranes with changing properties. Therefore, studying particle interactions with membranes of varying compositions and in different states could improve the predictability of biodistribution.

In our work, we want to focus on one particular membrane property, the membrane curvature. First, we want to give a brief introduction to this property. How should we picture the curvature of a membrane? To get a good idea, let's first consider a planar membrane. If we now press a spherical shape with the radius r_S onto this membrane, an invagination will form which corresponds to the negative shape of the sphere. The curvature K_m of the membrane section that is in contact with the sphere is then equal to the reciprocal of the square of r_S (Fig. 2A) [85]. This curvature is commonly referred to as gaussian curvature.

$$K_m = \frac{1}{{r_S}^2} \tag{15}$$

However, while the gaussian curvature is a suitable measure to characterize the shape of a membrane, what factor does indeed determine this shape? This factor is called spontaneous curvature and it can be thought of as an intended membrane shape that is continuously strived for by the actual membrane shape. One force contributing to this is the spontaneous curvature of the membrane's lipid components. This spontaneous curvature describes the tendency of individual lipid molecules to induce positively or negatively curved membranes (e.g., O/W- or W/O micelles, Fig. 2B) [86,87]. Next to the lipid components, also proteins attached to or intercalating the membrane also contribute to the overall spontaneous curvature [88].

This parameter is relevant for the interaction of nanoparticles with membranes, as any change in the membrane shape contrary to the direction dictated by the spontaneous curvature requires an energy input, referred to as bending energy. Since changes in membrane curvature occur during initial binding and further invagination of a particle at the membrane, the bending energy is a barrier to be overcome for these processes. In this context, fundamental scientific efforts have led to the realization that the height of this energetic barrier depends on the initial curvature of the membrane. It was found that a membrane curvature towards the particles reduces the bending energy to be supplied (Fig. 2C) [89–93]. Since the bending energy must be provided by the binding energy released during attachment, it follows that with a membrane curvature approaching the curvature of the binding particle, the binding energy to be applied approaches a minimum. Analogously, it can be concluded that for a given binding energy (e.g., for a given ligand attached to a particle), the bending energy to be overcome is lowest at the membrane whose curvature most closely matches that of the particle.

Finally, we want to propose a linkage between membrane curvature and the theoretical framework underlying the avidity of multivalent interactions. In doing so, we want to shed a light on the binding of ligand-functionalized particles, as these have been largely neglected in the previous investigation on the impact of membrane curvature. Let us consider a particle approaching a completely flat membrane (Fig. 2C sub-figure (A)) and a membrane corresponding to its surface curvature (Fig. 2C sub-figure (B)). What would the laws of avidity introduced in the previous section suggest in this case? It is reasonable to assume that the larger contact area will result in a higher number of ligands being located in close proximity to their receptors. Assuming the condition formulated in Eq. 11, it follows that a higher number i of bonds will form in this case, which is why process (B) can be assumed to be thermodynamically favorable (Eq. 12 and 13). Consider a third case (Fig. 2C sub-figure (C)), in which a particle encounters two membrane structures concurrently, one of which contains many membrane segments like the one in (B). The considerations presented above lead to the conclusion that there will be a preferential binding of the particle to the membrane with the curved segments.

Interestingly, such curved membrane segments are not just a purely theoretical construct. They have a biological pendant. For instance, clathrin-coated pits (CCPs) are spontaneously formed [94] morphological membrane entities in good correspondence with nanoparticles of a diameter of 50–150 nm [95]. Given the introduced theoretical framework of avidity and the effects of membrane curvature on particle attachment, we consider it conceivable that CCPs might act as binding hot-spots in the interaction of ligand-functionalized nanoparticles with cell membranes. First investigations of our group point in that direction [96].

4. Theory: Brief summary

The central take-home message of the theoretical considerations is that an accumulation of ligand-functionalized nanoparticles will preferentially occur in cells with higher receptor expression. This is the case as long as the favorable binding enthalpy transfer ΔH outnumbers the unfavorable decrease in entropy ΔS:

$$\Delta G = \Delta H - T\Delta S \tag{rep. Eq. 7}$$

This is the case since a process only runs voluntarily if the free Gibbs energy ΔG is negative. More detailed models of the Gibbs free energy for the specific case of multivalent interactions show that a main driver is

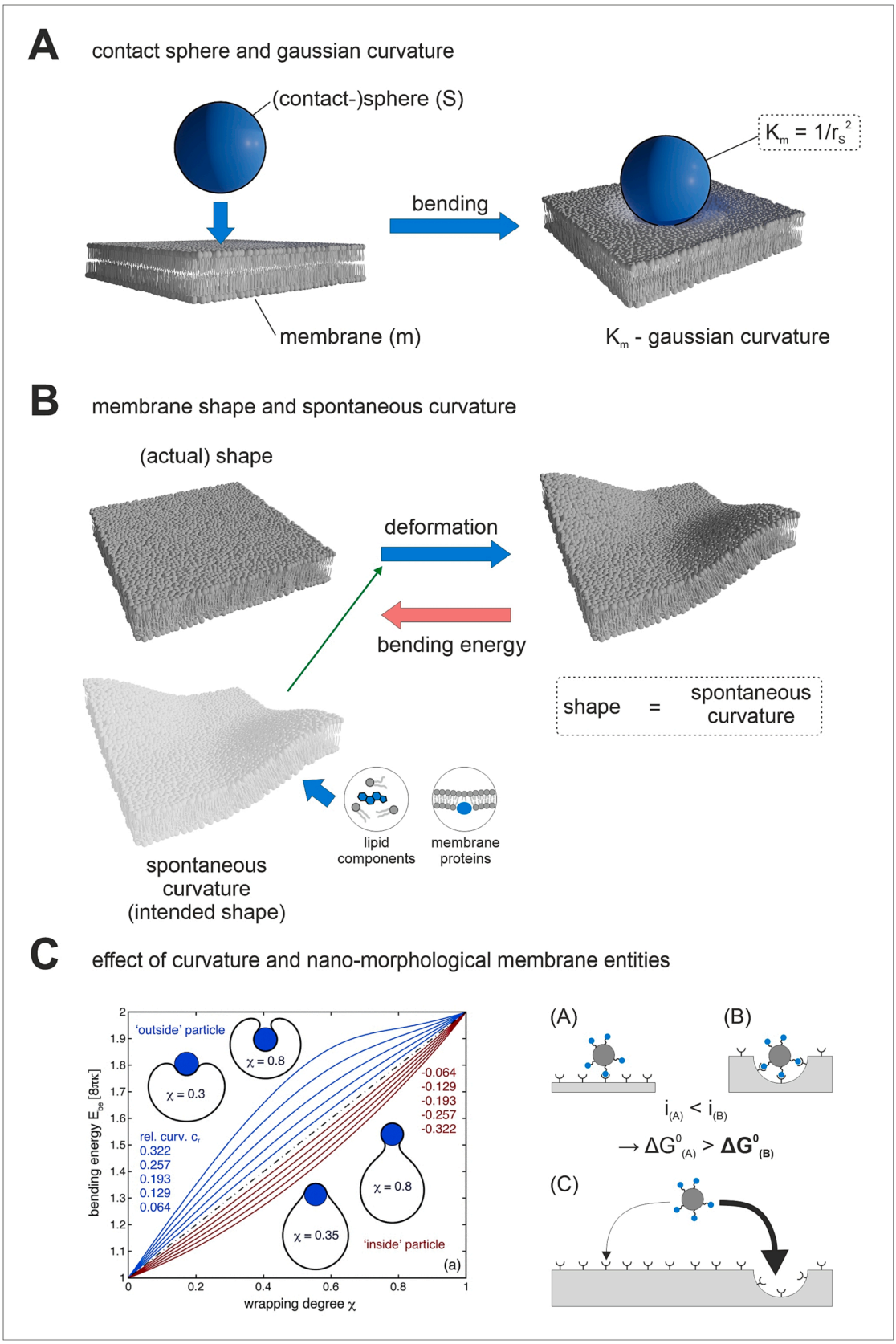

(caption on next page)

Fig. 2. Introduction to the concept of membrane curvature and how it affects particle-membrane interactions. (A) As a measure to characterize the curvature of a membrane, we introduce the gaussian curvature K_m. This parameter can best be understood by imagining a sphere lowering onto the membrane and forming an invagination. The gaussian curvature of the membrane in contact with the sphere (i.e., contact sphere) then is given by $K_m = 1/r_S^2$, where r_S is the radius of the contact sphere. (B) The driving force determining the shape of a membrane is the spontaneous, which can be understood as an intended shape of the membrane which the membrane aims to adopt. The spontaneous curvature itself is determined by the composition of the membrane as wells as by membrane attached and intercalating proteins. Most importantly, we note that any deformation contrary to the spontaneous curvature requires energy to be supplied to the system. This energy is referred to as bending energy. (C) This bending energy is key to understand the impact of membrane curvature on particle-membrane interactions, as it resembles a barrier to be overcome to allow particle attachment and further ingestion. It was found that a membrane curvature facing towards a particle (i.e., 'inside' particle) reduces the required bending energy. Data presented plots the bending energy barrier against the wrapped membrane fraction (χ, i.e., the proportion of particle surface in contact with membrane). Red curves represent 'inside' particles (i.e., membrane curved toward the particle), blue curves represent 'outside' particles (i.e., membrane curved away from the particle) (Reproduced from Ref. [93] with permission from the Royal Society of Chemistry) [93]. Combining the presented theoretical framework on avidity with the curvature dependence of particle binding, we conclude that membrane sections matching particle curvature could represent binding hotspots. This appears evident, due to lower Gibbs free energies suggesting preferential attachment. (For interpretation of the references to colour in this figure legend, the reader is referred to the web version of this article.)

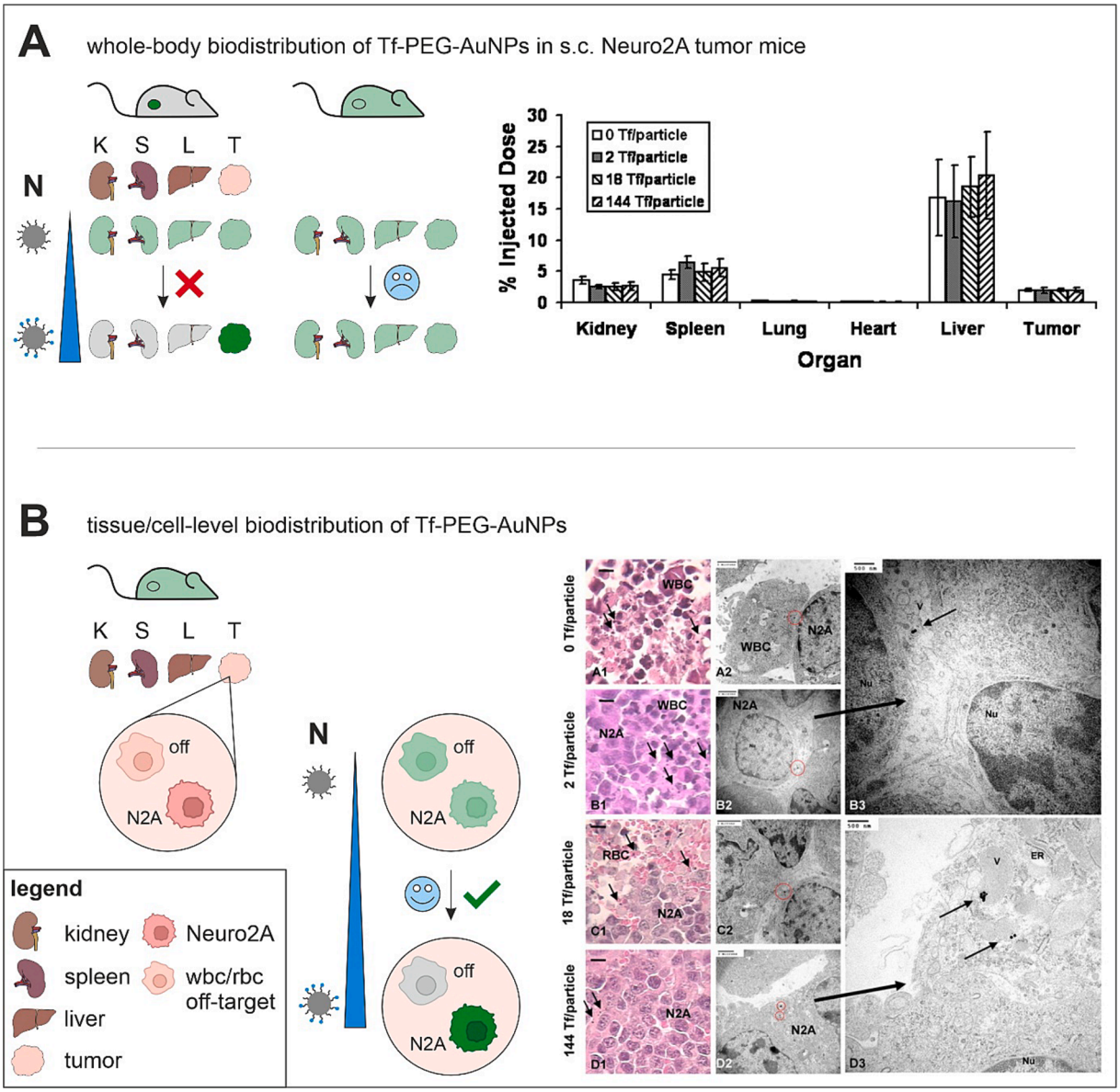

Fig. 3. In vivo biodistribution of transferring functionalized PEGylated Au-nanoparticles targeting transferrin receptor in Neuro2A tumor-bearing mice. (A) The study found no significant effect of ligand functionalization on whole-body biodistribution. Also, with increasing degree of particle functionalization, no increased uptake in tumor or reduced accumulation in off-target organs was observed. (B) However, it was observed that at the tissue level, at the highest level of functionalization studied, there occurred a directional accumulation of particles in tumor cells. At the same time, no particles were found in the non-cancer cells within the tumor. It can be concluded that the observations at the tissue level are largely in line with expectations based on the theoretical framework of avidity (Copyright (2019) National Academy of Sciences).

the valence of the interaction, i.e. the number of bond pairs formed. From this it can be deduced that close contact between the membrane and the particle surface could favor the binding ability of the particle. At such points, the valence of the interaction would be increased (Fig. 2C).

Finally, there is also a direct correlation between the thermodynamic parameter of the Gibbs free energy ΔG and the avidity expressed as the dissociation constant K_D:

$$\Delta G = RT\ln K_D \quad \text{(rep. Eq. 14)}$$

This correlation shows that a negative value of ΔG results in a value of $K_D \ll 1$. The equilibrium of this reaction is therefore far on the side of the reaction products, in our case the bound particle. In this case, we would expect a strong accumulation of particles in receptor-rich tissues. To investigate the correlation of avidity and biodistribution, we must therefore compare this expectation horizon with the available experimental observations.

5. Effects ligand functionalization and avidity on particle biodistribution

In the second main section of our work, we aim to review the literature available on the relationship between avidity and bio-distribution. To this end, we have consulted studies that investigate the in vivo distribution of ligand-functionalized nanoparticles, optimally still providing information on the avidity of the particle under investigation. Following, we present these studies and discuss their main findings relevant to our matter.

Choi et al. have prepared PEGylated gold nanoparticles (AuNP) functionalized with varying amounts of transferrin (Tf-PEG-AuNPs). These particles showed Tf functionalization level-dependent avidity to transferrin receptor (TfR)-bearing Neuro2A cells. Avidity was found in the low nM to pM range (17.5 Tf/AuNP: 1.06 nM; 144.3 Tf/AuNP: 0.13 nM).

In vivo tumor distribution was investigated in s.c. Neuro2A tumor bearing mice. Despite TfR overexpression confirmed via antiTfR-AF555 staining of Neuro2A cells, only very small amounts of administered Tf-PEG-AuNP doses accumulated in tumors (2–3 %). Moreover, the extend was independent of Tf-functionalization degree (Fig. 3A). In contrast, at the tissue level an increasing accumulation of Tf-PEG-AuNP in the Neuro2A target cells depending on the Tf content could be observed in the tumor. While unfunctionalized particles and particles with low Tf content were found mainly in leukocytes, higher Tf content resulted in targeted accumulation in Neuro2A cells (Fig. 3B).

The authors conclude from these observations that ligand functionalization is not suitable to positively influence whole-body biodistribution. They see the beneficial effect of targeted nanoparticles at the tissue level, where ligand functionalization can lead to accumulation in target cells [97].

A further study by Gu et al. investigated a nanoparticle based on poly (D,L-lactide-co-glycolide) (PLGA)-b-polyethylene glycol (PEG)-b di-block copolymers. Ligand decorated particles targeting prostate-specific membrane antigen (PSMA) were prepared by incorporating PLGA-b-PEG di-block-co-polymers additionally functionalized with A10 2′-fluoropyrimidine RNA aptamer (PLGA-b-PEG-b-Apt). Also in this study, the influence of ligand density was investigated by using different ratios of PLGA-b-PEG-b-Apt and PLGA-b-PEG-b to prepare nanoparticles. To allow quantification of nanoparticles in vivo, particles were prepared using tritium-labeled PLGA. In vivo biodistribution was investigated in s.c. LNCaP xenograft mouse models (Fig. 4).

While the proportion of the administered dose reaching the tumor was also very low in this case, increased accumulation in the tumor was observed with increasing ligand density over a certain range. The non-functional ligand particle was inferior to all other particles. Interestingly, also compared to the unfunctionalized nanoparticle. From this it can be concluded that the positive effects of functionalization with ligand-RNA are not exclusively due to unspecific effects (e.g., charge-mediated interactions). It is, however, further noteworthy that this effect inverts above a certain level of functionalization. The authors attribute this to a reduction of the PEG-related stealth effect [98–100] at higher levels of RNA aptamer functionalization. This explanation would also be coherent with the likewise increasing accumulation in liver and spleen at this degree of functionalization. Additionally, ligand density was directly proportional to liver accumulation of the particles. Here, a degree of functionalization could be found at which the undesired liver accumulation had already decreased significantly, while tumor accumulation reached its maximum.

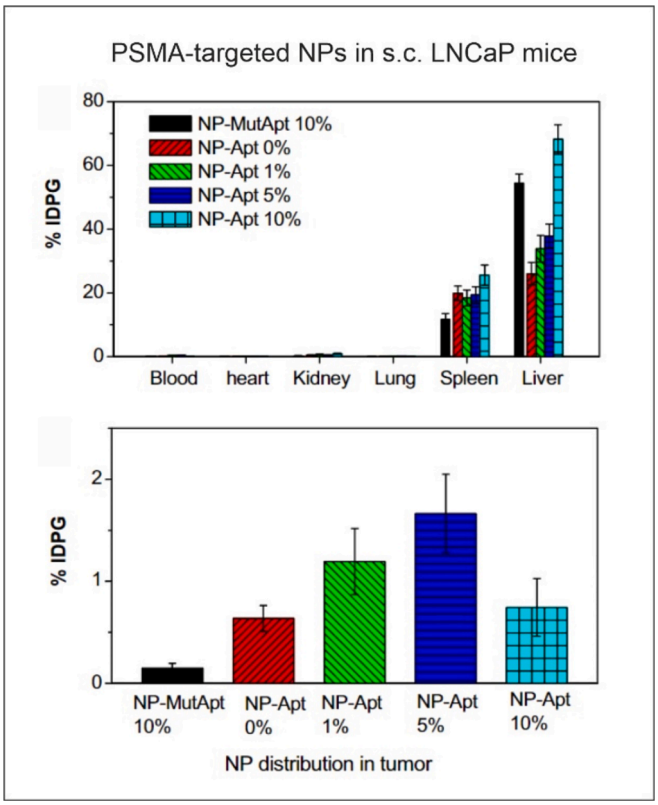

Fig. 4. In vivo biodistribution of RNA-aptamer functionalize PLGA-b-PEG nanoparticles targeting prostate-specific membrane antigen (PSMA) in LNCaP tumor-bearing mice. The whole-body biodistribution study showed that most particles accumulate in the liver and in the spleen. The amounts increase in both organs with increasing degree of functionalization. It is specifically noteworthy that there are only minor differences between ligand functionalized particles and particles carrying a non-functional surrogate of the ligand. This implies that the accumulation in these organs did not occur due to a specific ligand-receptor interaction, but rather was the result of an unspecific mode of transport. The cascade leading on this accumulation has been described in detail in the literature [102–104]. (Copyright (2008) National Academy of Sciences).

The authors concluded that there is a narrow window for the degree of functionalization at which an optimal targeting effect is achieved and that this window must be determined individually for each particle system [101].

Kirpotin et al. made similar observations with a distinct nanoparticle platform. Designing a PEG-chain functionalized liposome decorated with anti-HER2 monoclonal antibody fragments they aimed for solid tumor targeting. Biodistribution was investigated in s.c. BT-474 or MCF-7 tumor bearing mice.

For investigation of biodistribution, unfunctionalized and HER2-targeted liposomes were radio-labeled via encapsulation of ^{67}GA-DTPA chelate. A method that the group has thoroughly validated in terms of a possible influence of the labeling on pharmacokinetics and a possible leakage of the chelate [105].

However, also in their case, only a low proportion of the administered liposome dose reached the desired tumor tissue in s.c. BT-474 tumor bearing mice (7–8 %). Again, no significant effect of ligand functionalization on whole-body biodistribution was detected in this study. Specifically, no increased accumulation in tumors of HER2-targeted liposomes was found compared with unfunctionalized controls (Fig. 5A). It must be emphasized that the authors had investigated the in vitro uptake of HER2-targeted and control liposomes in HER2 overexpressing SK-Br-3 cells and found a superior uptake of the anti-HER2 particles. Regrettably, only the functionalized liposome was compared with an unfunctionalized control. An investigation of the influence of increasing avidity with increasing valency of the particle was therefore unfortunately not possible.

One merit of the Kirpotin et al. study over Choi et al. is that the former examines bio-distribution at the tissue level in more detail by employing a quantitative method. This was done using flow cytometry

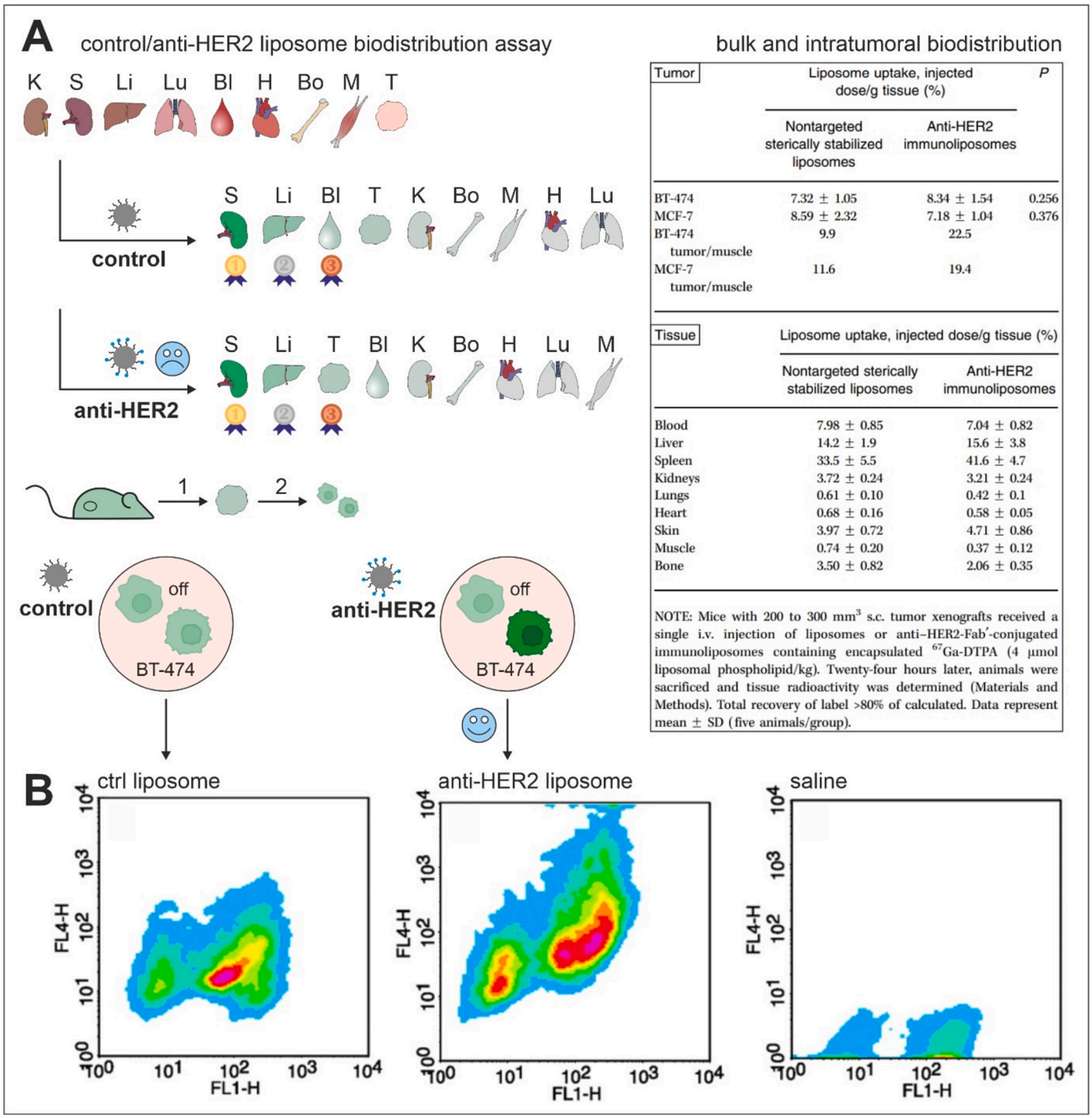

bulk and intratumoral biodistribution

Tumor	Liposome uptake, injected dose/g tissue (%)		P
	Nontargeted sterically stabilized liposomes	Anti-HER2 immunoliposomes	
BT-474	7.32 ± 1.05	8.34 ± 1.54	0.256
MCF-7	8.59 ± 2.32	7.18 ± 1.04	0.376
BT-474 tumor/muscle	9.9	22.5	
MCF-7 tumor/muscle	11.6	19.4	

Tissue	Liposome uptake, injected dose/g tissue (%)	
	Nontargeted sterically stabilized liposomes	Anti-HER2 immunoliposomes
Blood	7.98 ± 0.85	7.04 ± 0.82
Liver	14.2 ± 1.9	15.6 ± 3.8
Spleen	33.5 ± 5.5	41.6 ± 4.7
Kidneys	3.72 ± 0.24	3.21 ± 0.24
Lungs	0.61 ± 0.10	0.42 ± 0.1
Heart	0.68 ± 0.16	0.58 ± 0.05
Skin	3.97 ± 0.72	4.71 ± 0.86
Muscle	0.74 ± 0.20	0.37 ± 0.12
Bone	3.50 ± 0.82	2.06 ± 0.35

NOTE: Mice with 200 to 300 mm^3 s.c. tumor xenografts received a single i.v. injection of liposomes or anti–HER2-Fab′-conjugated immunoliposomes containing encapsulated ^{67}Ga-DTPA (4 μmol liposomal phospholipid/kg). Twenty-four hours later, animals were sacrificed and tissue radioactivity was determined (Materials and Methods). Total recovery of label >80% of calculated. Data represent mean ± SD (five animals/group).

Fig. 5. In vivo biodistribution of anti-HER2-Mab functionalized PEGylated liposomes targeting human epidermal growth factor receptor 2 (HER2) in BT-474 and MCF-7 tumor-bearing mice. (A) The findings of Kirpotin et al. are essentially consistent with the observations made by Choi et al. This study, however, included a larger number of off-target organs. Yet still no substantial effect of ligand functionalization was found, regarding whole-body biodistribution. (B) The work of Kirpotin et al. further adds value, as a quantitative method was used to measure particle distribution at the tumor levels. For this, (1) tumors were extracted and (2) disaggregated to allow single cell analysis via flow cytometry (Adapted from Cancer Research, 2006, 66/13, 6732–6740, Kirpotin et al., Antibody Targeting of Long-Circulating Lipidic Nanoparticles Does Not Increase Tumor Localization but Does Increase Internalization in Animal Models, with permission from AACR).

analysis of extracted disaggregated tumor after i.v. treatment of tumor bearing mice with HER2-targeted or control liposomes. For detection ADS645WS was encapsulated into liposomes. To distinguish tumor and off-target cells, EpCAM on tumor cells was stained using anti-EpCAM Mab-FITC. Additionally, gold-tagged liposomes were visualized in fixed tumor tissue samples via silver enhancement and imaged using bright-field and dark-field microscopy. In summary, intra-tumor biodistribution analysis showed a clear preferential uptake of anti-HER2 liposomes compared to control liposomes in tumor cells (Fig. 5B).

The authors conclude that the mechanism behind the improved efficacy of ligand-functionalized particle therapy differs from the classical understanding of targeted nanoparticles for their system. In their view, instead of an organ/tumor-specific accumulation, a cell-specific accumulation at the tissue level is in the foreground [106]. To summarize, while a base-level of particle uptake was found in cancer as well as non-cancer cells for non-targeted particles considerably above the level of the particle-free control, anti-HER2 liposomes showed a significantly higher uptake in cancer cells. Therefore, evidence for the fundamental

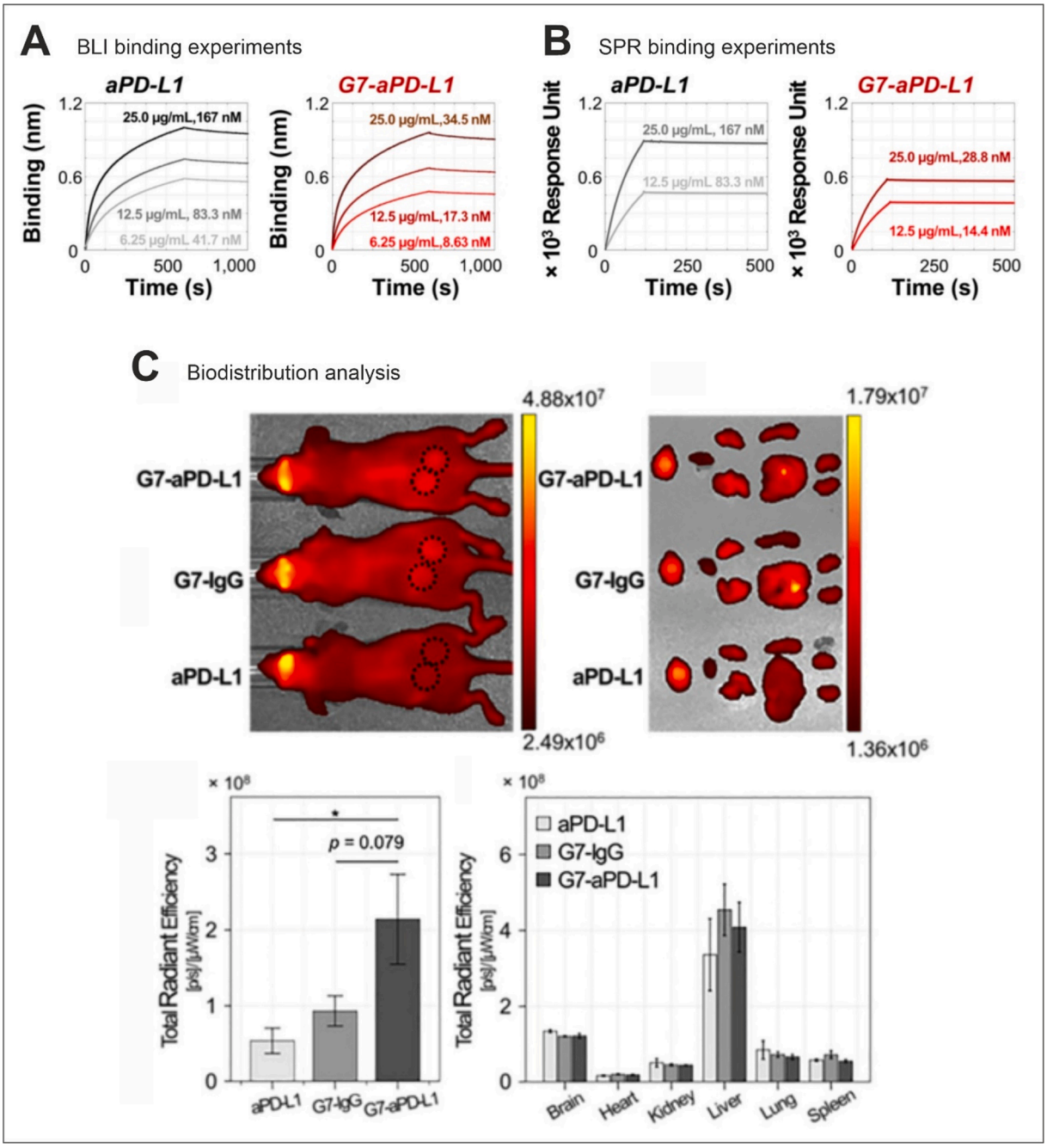

Fig. 6. In vivo biodistribution of aPD-L1 functionalized PAMAM dendrimers targeting programmed death ligand 1 (PD-L1) in MOC1 tumor bearing mice. The study presented by Bu et al. is one of the few cases where particle avidity data is presented alongside a whole-body biodistribution experiment. The authors conducted (A) biolayer interferometry (BLI) as well as (B) surface plasmon resonance (SPR) binding experiments, yielding dissociation constants K_D in the fM range with an avidity-gain of the multivalently functionalized dendrimer over the free ligand of one order of magnitude. (C) However, the observations the observed biodistribution of the free ligand and the multivalent entity possessing a demonstrated avidity-gain over the free ligand did not differ significantly. A higher accumulation of the ligand functionalized particle was observed compared to the free ligand. The differences observed compared to the non-targeted particle were not found significant (Reprinted with permission from Nano Letters, Bu et al., An Avidity-Based PD-L1 Antagonist Using Nanoparticle-Antibody Conjugates for Enhanced Immunotherapy, Nano letters 20 (2020) 4901–4909, (2020), American Chemical Society).

laws of avidity to be applicable on the tissue-level was generated.

Another very informative study on this subject was conducted by Bartlett et al. Here, positron emission tomography (PET) and bioluminescent imaging were used to investigate the in vivo biodistribution. As Choi et al. they aimed for TfR targeting in Neuro2A tumors.

In this study, a nanoparticle system based on complexes formed from cyclodextrin-containing polycations and siRNA molecules was investigated. Addition of adamantane-PEG polymers functionalized with Tf yielded the ligand functionalized TfR-targeted nanoparticle. To enable PET-based biodistribution studies, a 1,4,7,10-tetraazacyclododecane-1,4,7,10-tetraacetic acid (DOTA) 5′-modified siRNA labeled with ^{64}Cu was employed [107]. Studies were conducted on mice bearing s.c. Neuro 2A tumors modified to express luciferase.

Although the authors observed similar bulk biodistribution and tumor localization of untargeted and Tf functionalized particles in micro-PET/CT imaging, therapeutic efficacy of targeted nanoparticles was found to be superior compared to control particles. This was demonstrated by a significantly higher reduction in luciferase activity after treatment with Tf functionalized particles compared with unfunctionalized particles. The proportion of the dose reaching the tumor was again low and was not significantly affected by Tf functionalization of the particles.

Unfortunately, the study did not experimentally investigate the intratumoral particle distribution. However, a very insightful compartment-based model is presented that demonstrates at which point ligand-functionalized particles can play to their strengths. The authors see this possibility primarily in the case of particles that can rapidly diffuse from interstitium back into the plasma. Here, ligand functionalization enables a significant improvement in cellular uptake [108].

The study of Bu et al. investigated immune-checkpoint inhibitor carrying dendrimers (G7-aPD-L1) targeting PD-L1 for their efficacy in cancer immunotherapy. It must be emphasized that in this study nanoparticle binding kinetics were characterized very thoroughly. For this, three distinct methods were applied. Biolayer interferometry (BLI), surface plasmon resonance (SPR), and atomic force microscopy (AFM) were conducted to determine dissociation constants (K_D) as well as association and dissociation rate constants (k_{on} an k_{off}). In summary, K_D for G7-aPD-L1 conjugate was found in a fM range (BLI: $K_D = 8.5 \times 10^{-11}$ M; SPR: $K_D = 6.6 \times 10^{-11}$ M). This corresponds to an avidity gain of about one order of magnitude compared to aPD-L1 (BLI: $K_D = 9.6 \times 10^{-10}$ M; SPR: $K_D = 3.8 \times 10^{-10}$), which was mainly caused by an increase in k_{on} (BLI: $2.38 \times 10^5 \rightarrow 1.10 \times 10^6$ $M^{-1}s^{-1}$; SPR: $5.54 \times 10^4 \rightarrow 3.61 \times 10^5$ $M^{-1}s^{-1}$) with less prominent changes in k_{off} (BLI: $2.75 \times 10^{-4} \rightarrow 6.79 \times 10^{-5}$ s^{-1}; SPR: $2.18 \times 10^{-5} \rightarrow .88 \times 10^{-5}$ s^{-1}) (Fig. 6 A and B).

Interestingly, this observation is in direct contradiction with the results of Wang et al. who found for EC1-functionalized ErbB2-targeting micelles that superior avidity of the multivalent entity over free EC1 was due to a reduction of k_{off} (SPR: $6.21 \times 10^{-2} \rightarrow .1 \times 10^{-3}$ s^{-1}), whereas k_{on} showed no clear trend and underwent only minor changes (SPR: $4.84 \times 10^3 \rightarrow 8.42 \times 10^3$ $M^{-1}s^{-1}$) [109]. Unfortunately, this particle system was not tested in vivo for the influence of its avidity on biodistribution. For this reason, no conclusive statement on the influence of the mechanism underlying nanoparticle avidity gain on biodistribution is possible.

Regarding studies conducted by Bu et al., little to no differences can be made out comparing G7-aPD-L1 and the free binding entity aPD-L1 regarding distribution over the major off-target organs. The dose of G7-aPD-L1 accumulated in the tumor, however, was significantly higher compared to aPD-L1. As a control for passive tumor targeting, the authors included an IgG dendrimer conjugate (G7-IgG). Also compared to this control, there is no significant difference in whole-body biodistribution. In terms of dose accumulated in tumor, G7-aPD-L1 appears superior, but the difference is not statistically significant [110] (Fig. 6C).

An outstanding fundamental work in this context was presented by Schmidt et al. Based on a mechanistic compartmental model [111], the authors derive predictions on affinity-dependence of tumor targeting in excellent overlay with experimental observations. In agreement with the experimental data [112], the model finds a plateau-like dependence in which the desired uptake into the tumor decreases in a step-like manner once the affinity falls below a critical value. The authors go further and provide another analysis highly relevant for the question of the influence of avidity of ligand-functionalized nanoparticles on their biodistribution.

In a simulation, they parallelly investigate the influence of (a) molecular weight and (b) the affinity of a binding entity on the percentage of dose per gram delivered to the tumor tissue. Using the rule of thumb to estimate the hydrodynamic diameter R_{mol} based on the molecular weight $M_W = 1.32R_{mol}^3$, it can be concluded from this analysis that the avidity of nanoparticles > 50 nm has hardly any influence on this parameter and that the accumulation in the tumor only decreases at very low avidities $K_d > 100$ nM.

In their conclusions, the authors highlight this observation, that for molecules exceeding a certain size, antigen targeting has little or no effect on tumor uptake, as one of the most intriguing findings of their study [113]. However, we must emphasize that Schmidt et al. primarily consider antibodies in their work and that studies on the transferability of their findings to nanoparticles are not yet available in literature.

Another contribution to fundamental understanding of the interplay between the avidity of a ligand-functionalized nanoparticle and its biodistribution is provided by Zern et al. In their work, they make the argument that the ratio of specific to nonspecific accumulation (i.e., ratio of particle amount in target to off-target tissue) should be considered as a parameter of success for targeted nanoparticles. This target/off-target ratio should take precedence over absolute exposure of target tissues to the administered nanoparticle. With this shift in focus, the authors highlight the often-overlooked problem of lower-level expression of addressed target structures (e.g., receptors) in non-target tissues.

They investigated an intercellular adhesion molecule-1 (ICAM-1)-antibody decorated poly(4-vinylphenol) (PVPh) nanoparticle (anti-ICAM-1/NP) additionally radiolabeled with ^{124}I to allow PET/CT imaging. This particle was administered to untreated C57BL/6 mice to determine biodistribution of anti-ICAM-1/NP at basal ICAM-1 expression levels. To investigate the effect of ICAM-1 overexpression in lung vasculature on anti-ICAM-1/NP biodistribution, mice were challenged via intratracheal installation of lipopolysaccharide (LPS). Ligand density on PVPh nanoparticles was tuned by replacing a portion of ICAM-1 antibodies with IgG as control (Fig. 7A and C).

They find that already in untreated mice, uptake of anti-ICAM-1/NP in the lungs increases with increasing ligand density. An anti-ICAM-1/NP with 50 antibodies per particle was found to not differ significantly from IgG control nanoparticle regarding lung uptake. Upon LPS challenge, uptake increases as expected. However, while only a 2.4-fold increase is observed for the high-avidity anti-ICAM-1/NP (200 antibodies per particle), the low-avidity anti-ICAM-1/NP (50 antibodies per particle) shows a 5.3-fold increase in uptake. Since free anti-ICAM-1 antibody also shows a 2.4-fold higher uptake upon LPS treatment, one cannot conclude a beneficial influence of multivalent functionalization in the case of high-avidity anti-ICAM-1/NP in this regard (Fig. 7B). The study of Zern et al. is particularly valuable to our matter, as via a lipopolysaccharide (LPS) challenge the author varied the receptor density in the target organ. In this way a significant impact of the receptor density could be shown.

With their focus on a diagnostic application to detect pulmonary inflammation, the authors conclude that the reduction in avidity achieved via decreasing ligand density, was beneficial regarding functionality of their particle [114]. It should be noted, however, that the avidity of anti-ICAM-1/NP was not quantified (e.g., via SPR or BLI). Furthermore, regarding a conceivable transfer of the findings to therapeutic applications, it should be noted that with low-avidity anti-ICAM-1/NP, a recognizable accumulation in the spleen persists even after LPS treatment. This was prevented when increasing ligand density to 200 antibodies per particle. In this way, the study of Zern et al. indeed provides

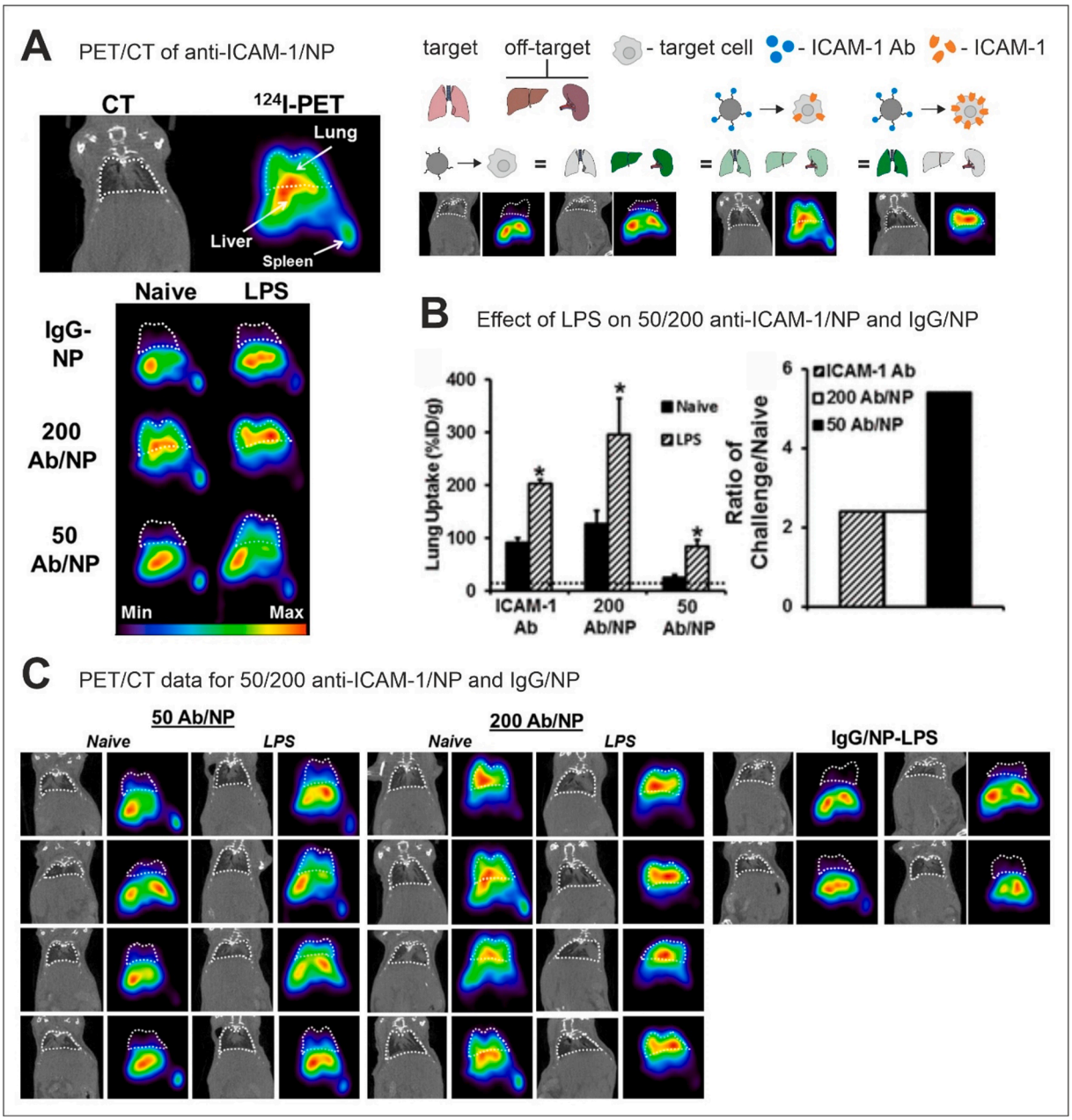

Fig. 7. In vivo biodistribution of ICAM-1-Ab functionalized PVPh nanoparticles targeting intercellular adhesion molecule 1 (ICAM-1) in pulmonary vasculature of endotoxin-challenged mice. (A) Using a combined PET/CT imaging approach, Zern et al. followed the whole-body biodistribution of their particle system. (B) The authors found that the uptake of the free ligand was increased upon LPS challenge to the same degree as the high-valency particle. A significantly higher effect of the LPS-induced increase of receptor density was found for the low valency particle. (C) Distribution data of all animals studied (Reprinted with permission from ACS nano, Zern et al., Reduction of nanoparticle avidity enhances the selectivity of vascular targeting and PET detection of pulmonary inflammation, ACS nano 7 (3), S. 2461–2469, (2013), American Chemical Society).

evidence for the transferability of the basic laws of avidity to the biodistribution of ligand-functionalized particles.

In an earlier study the same group investigated PVPh-based nanoparticles addressing a variety of target structures, all endothelial markers in pulmonary vasculature. These were platelet-endothelial cell adhesion molecule-1 (PECAM-1), thrombomodulin, and PV1. In this work the authors did not vary the ligand density on their particles. No significant effect of ligand functionalization on bulk biodistribution was found, but a massively increased uptake in the lung was detected [115]. This observation shows that even without a change in bulk biodistribution, ligand functionalization can lead to greatly enhanced uptake in the target tissue. This finding suggests that bulk biodistribution and distribution at the cellular level should be considered separately. The advantage of ligand functionalization could already lie in an improved cellular uptake in the target tissue (e.g., compared to an extracellular accumulation of non-targeted particles). This would not necessarily be apparent if only bulk biodistribution were considered.

Frigell et al. investigated the suitability of multivalently ligand functionalized nanoparticles for targeted delivery to the central nervous system. For this purpose, glucose-coated gold nanoparticles (GNPs) were designed to carry opioid peptides as targeting ligands. Two peptides were tested with the intention to improve blood–brain barrier passage. Particles were administered to male Sprague–Dawley rats via lateral tail veins. To allow analysis of whole-body biodistribution, a chelator for the positron emitter ^{68}Ga was additionally attached to the GNPs. Particle distribution was assessed using whole-body PET imaging (Fig. 8A) as

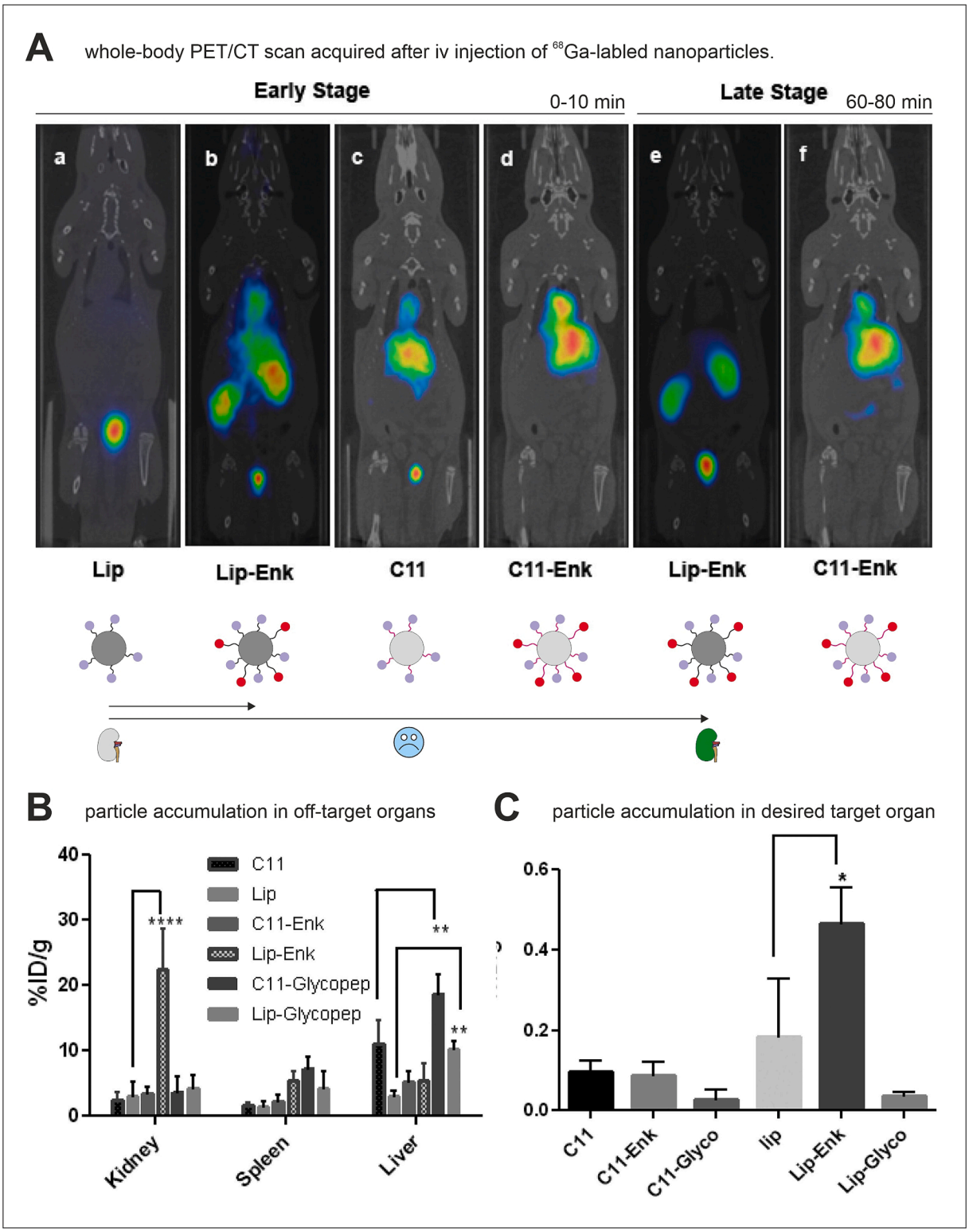

Fig. 8. In vivo biodistribution of neuropeptide functionalized glucose-coated Au-nanoparticles targeting opioid receptors to achieve blood–brain barrier passage in Sprague–Dawley rats. (A) The study investigated biodistribution for particles carrying one of two ligands (Enk/Gylcopep) attached via one of two linkers (Lip/C11) using PET/CT scans acquired shortly after particle administration (0–10 min) and after an extended time (60–80 min). (B) Overall, accumulation in the off-target organs was highly variable, with ligand functionalization tending to increase this accumulation. (C) The accumulation in the intended target organ was low. Only for one ligand- linker combination, a beneficial effect of ligand functionalization was found (Reprinted with permission from Journal of the American Chemical Society, Frigell et al., 68 Ga-labeled gold glyconanoparticles for exploring blood–brain barrier permeability: preparation, biodistribution studies, and improved brain uptake via neuropeptide conjugation, Journal of the American Chemical Society 136 (1), 449–457., (2013), American Chemical Society).

well as gamma counter analysis of extracted organs.

Regarding the impact of the targeting ligand on particle biodistribution, the authors report ligand functionalization to increase accumulation in the kidney (Fig. 8B). Regarding the desired accumulation in the brain, for both ligand-functionalized and unfunctionalized particles only minor proportions of the initial doses were found here. However, one of the two tested peptides induced a 2.5-fold increase of particle accumulation in the brain Fig. 8C). It is surprising that only one of the two peptides tested showed an effect. This could be because the peptide that shows no effect lacks the Tyr-Gly-Gly-Phe amino acid sequence which is considered essential for opioid receptor binding and activation [116,117].

Wang et al. synthesized an RNA-oligonucleotide based nanoparticle platform (three-way junction RNA, 3WJ) which was labeled via hydrogen-tritium-exchange conducted on the oligonucleotides themselves. The authors furthermore prepared fluorescently labeled nanoparticles by introducing the AFDye 647 fluorophore. Two targeting ligands were evaluated, the first being folic acid (3WJ-FA) targeting the folate receptor and the second being the CL4 RNA aptamer (3WJ-CL4) targeting the EGF receptor. In vivo pharmacokinetic and biodistribution studies were carried out by administering 100 μL of a 20 μM nanoparticle dispersion to mice bearing KB or MDA-MB-231 tumors via tail vein injection. While KB tumors strongly express the folate receptor [118], MDA-MB-231 tumors are used as a model for cancers strongly overexpressing EGFR [119,120]. Next to targeted particles (3WJ-FA and 3WJ-CL4), unfunctionalized 3WJ particles and PBS were applied as controls.

Firstly, the authors employed fluorescently labeled nanoparticles to evaluate the binding avidity of 3WJ-FA and 3WJ-CL4 to their respective target cells. Particle concentration-dependent increase of fluorescence was recorded in flow cytometry experiments. For the avidity of 3WJ-FA to KB cells a K_D of 322.8 nM was found. For the interaction of 3WJ-CL4 with MDA-MB-231 cells the K_D was found to be 72.1 nM.

In mice sacrificed 4 or 8 h after nanoparticle administration, the authors found 5 % of 3WJ-FA and 3 % of 3WJ-CL4 accumulated in the tumor. For 3WJ-FA tumor accumulation was superior to that of unfunctionalized control particles at both time points (5 % 3WJ-FA vs. 3 % 3WJ at 4 and 8 h), while for 3WJ-CL4 this was only the case after 8 h (3 % 3WJ-CL4 vs. 2 % 3WJ at 4 h: ns.; and 1 % at 8 h). For both investigated particle species, ligand functionalization had only minor effects on particle accumulation in off-target organs. The authors also performed in vivo fluorescence biodistribution studies, which yielded results similar to the radio-label based experiments. [121].

Putting the observations of Wang et al. into perspective with the general concept of multivalency-determined avidity of ligand functionalized nanoparticles, it is surprising that the particle with inferior avidity appears to outperform the one with a higher avidity to its target cell. 3WJ-FA shows an overall higher tumor accumulation which is consistently superior to unfunctionalized control particles. Also, 3WJ-FA shows a more favorable tumor to off-target ratio in the case of tumor/heart-tissue distribution compared to 3WJ-CL4. Regrettably, the authors did not vary the degree of ligand functionalization for either of their particles.

In their study Ganesh et al. investigate the biodistribution previously prepared and characterized by the group. The particle design is based on polyethyleneglycol (PEG) and polyethyleneimine (PEI) polymers linked to a hyaluronic acid (HA-PEG and HA-PEI) backbone. These polymers were found to possess a self-assembling ability inducing the formation of 50–80 nm nanoparticles [122].

For the study on biodistribution, additionally to cisplatin and a siRNA duplex intended to exploit a beneficial effect on cisplatin-resistant tumors the authors encapsulated the near infrared (NIR) dye indocyanine green to measure whole-body distribution. Due to its HA functionalization, a CD44 directed targeting effect was expected. The biodistribution was examined in human non-small cell lung cancer A549 and A549/DDP bearing mice after three injections via the tail vein administered over three days. Next to this experiment, the authors performed further biodistribution studies comparing tumors showing a high CD44 (i.e., A549 and A549/DDP) [123] expression with tumors known to express lower levels of CD44 (i.e., H69 and H69AR) [124]. NIR signal was recorded in mice 10 min, 4, 10, and 24 h after administration. While distribution initially occurred throughout the entire body in all tumor models, accumulation in tumor tissue was evident after 4 h in A549 and after 10 h in A549/DDP. In H69 and H69AR, no accumulation in tumor tissue was seen during the entire observation period.

As another study of interest for distribution, the authors also quantified siRNA in off-target organs and in tumor tissue using a PCR technique. A strong decrease of siRNA in the liver tissue was found over the course of 24 h. The proportion of the initial dose administered fell from 33.4 % (1 h) to 13.4 % (24 h). A similar pattern was observed for the spleen tissue, which contained 22.8 % of the initial dose after 1 h and 17.4 % after 24 h. At the same time, the proportion of initial dose found in tumor tissue increased from 0.5 % to 0.9 %. All changes were found to be statistically significant. While these observations are indicative of directional accumulation, it must be kept in mind, however, that they could also have resulted in part from degradation of siRNA by nucleases. [125].

Interestingly, the particle studied here accumulated in tumor tissue over time, during which the amount of particle present in off-target organs decreased significantly. Unfortunately, due to the particle design in which the avidity dictating moiety HA was also a part of self-assembling polymer backbone, it was not possible to vary ligand density or to investigate unfunctionalized particles in control experiments.

Akers et al. investigated perfluorocarbon-based nanoparticles which where functionalized with cRGD to enable $\alpha_v\beta_3$-integrin targeting. The particle surface was further functionalized with cypate-C18 (cypate–PFC-tNPs) to allow NIR-based detection of in vivo distribution in living mice tumor models. Whole-body biodistribution was assessed in male nude NCr mice bearing luciferase-transfected 4 T1 mouse mammary carcinoma cell (4T1luc) derived tumors. Regarding the improvement of tumor specific particle accumulation due to ligand functionalization the authors report a superior tumor-to-muscle distribution ratio for targeted nanoparticles compared to unfunctionalized control (6.9 to 3.0) in ex-vivo measurements. Unfortunately, in the whole-body imaging in this study, the targeted nanoparticle was compared only with a small-molecule cypate-cRGD compound and not with the unfunctionalized particle. Also, because the authors did not quantify the fraction of nanoparticle dose arriving in the tumor and have done hardly any detailed investigation of the distribution of particles into off-target organs (e.g., over time, comparison of targeted/non-targeted particles), it is difficult to assess the influence of ligand functionalization overall. The authors, however, found superiority of the small-molecule compound compared to the particle (8.1 to 6.9 tumor-to-muscle distribution ratio). [126].

This observation makes a simple transferability of the basic laws governing avidity to the case of biodistribution of ligand-functionalized nanoparticles questionable. Since these laws would suggest that the avidity of a multivalent entity is far superior to the single ligand affinity, this study thus suggests that factors act on the distribution of the particle which counteract the positive effect of multivalent functionalization.

6. Discussion

In the first part of this work, we introduce the concept of avidity and review literature providing evidence on what factors affect this property and how this concept translates to the case of nanoparticle-cell membrane interactions. In doing so, we were able to derive a general hypothesis about the distribution of ligand-functionalized nanoparticles in an environment with varying receptor densities, suggesting accumulation at high-receptor densities. Ultimately, the aim of this work was to investigate whether the experimentally found bio-distribution follows this hypothesis. Thus, whether there is a correlation between avidity and

bio-distribution. We also introduce the impact of membrane curvature on particle-membrane interactions, asking the question for the transferability of the described relations to the case of a ligand-functionalized nanoparticle. Already from these reflection on fundamental principles, approaches for further investigations can be derived. The available literature, for instance, provides evidence that different particle systems may differ in the mechanism underlying their avidity. Thus, it appears that the avidity can result from both, accelerated association (↑ k_{on}) and slowed dissociation (↓ k_{off}) [65,109,110]. As to the question of what influence the presence of one or the other mechanism has on the biodistribution of a nanoparticle, there is, to the best of our knowledge, no evidence available.

Summarizing the findings of the studies presented in the second part of the paper, it must be concluded that a clear assessment of the correlation of avidity and biodistribution is hardly possible based on presently available data. This is due to the fact that studies are lacking that have systematically investigated the biodistribution of a constant particle system with an avidity that varies over a quantified range. One reason for this is the all too understandable fact that in application-oriented research projects, it is primarily the most promising particle systems that are further investigated in in vivo experiments. Particles with poorer in vitro binding properties are not pursued further. However, this focus has led to a relevant knowledge gap regarding our understanding of nanoparticle interactions with biological systems that may inhibit the rational development of nanotherapeutics. In this context, our review points out an existing need for basic research on avidity-biodistribution correlation.

With regard to the excellent review by Kumar et al., it must be concluded that in the studies considered for our literature review, ligand functionalization did not lead to a significant deviation in the distribution across the organs (Table 1) compared to the expected values for the corresponding technology platform (Table 2) [146].

From the authors' perspective, only three of the relevant papers consulted for this review demonstrated directional accumulation of nanoparticles (Tables 1 and 3). Whereby, by directed accumulation we imply an accumulation of particles over time in the desired target tissue with simultaneous depletion in off-target tissues or organs. Only the works of Zern et al., Wang et al., and Ganesh et al. satisfy this strict interpretation of the term. To evaluate the question about decisive influencing factors for a directed biodistribution, it is worthwhile to consider in which properties the particles investigated in these studies differ from others. Thus, it is particularly noteworthy that with the work of Ganesh et al. the particle system associated with the ligand possessing the lowest receptor affinity is among the most successful systems. While this fact may be surprising at first, considering the basic principles of multivalency-induced avidity, it is consistent with previous theoretical considerations [147–149] and experimental observations [150–153]. Here, it has been reported that a lower affinity of the ligand used for functionalization leads to a higher target organ specificity of the resulting particle. A factor possibly causative of this circumstance can be deduced when taking a closer look at the "real-world" situation of nanoparticle-membrane interactions. Here, the initial binding of the particle already brings many ligands into close proximity to receptors. Once several ligand-receptor bonds have been formed, it is very likely, especially with high-affinity ligands, that even if individual ligands dissociate, they will quickly bind a receptor again due to the spatial proximity. It has been described that this phenomenon can lead to a practically irreversible binding of multivalent entities [46,154,155].

Furthermore, we find it remarkable that the study of Zern et al. is the only one in which an increasing avidity with particle valency could be demonstrated, which in turn led to a positive influence on the whole-body biodistribution. It should be emphasized that the targeted structure in this case was not a tumor tissue. This allows the hypothesis that factors typical of tumor environments counteract the targeted accumulation of ligand-functionalized nanoparticles. Cancer specific challenges in targeted nanoparticle delivery have very recently been reviewed by

Table 1
Investigated model systems and effect of ligand functionalization on particle biodistribution. The table provides an overview of the tissues or tumor models addressed with targeted particles in the studies consulted for this review. As a key parameter for describing the performance of the particle systems studied, we provide an overview of the dose fractions that reached the desired target tissue for both targeted (t) and non-targeted particles (nt). Also presented is whether a significant effect by ligand functionalization on whole-body biodistribution or tissue-level distribution was observed. In addition, for studies in which active compounds were encapsulated, we considered an improvement in therapeutic efficacy that may have been present (↑ - improvement, → - no significant change, ↓ - deterioration; arrows in brackets indicate conclusions subject to certain limitations). An improvement in whole-body biodistribution was considered as given when a higher proportion of the applied nanoparticle dose is found in the target organ, while the proportion in non-target organs is significantly reduced. Similarly, an improvement at the tissue level was given if the proportion of particles in target cells (e.g., tumor cells) increased and/or the proportion of particles in off-target cells decreased. Abbreviations and cell classifications: A549 - adenocarcinoma human alveolar basal epithelial cells, $A549^{DDP}$ - cisplatin-resistant A549, BT-474 - invasive ductal mamma-carcinoma cells, H69 - epithelial lung carcinoma cells, H69AR - doxorubicin-resistant H69, ID - initial dose, ID/cm^3 - initial dose per cm^3 tissue, ID/g - initial dose per g tissue, KB - adenocarcinoma endocervix cells, LNCaP - epithelial prostate carcinoma cells, MCF-7 - adenocarcinoma mamma cells, MDA-MB-231 - adenocarcinoma mamma cells, MOC1 - mouse oral squamous cell carcinoma, n.d. - no data available, Neuro2A - Neuroblastoma neuroblast cells, NSCLC - non-small-cell lung cancer, (n)t. - (non)targeted particle, TRE - total radiant efficiency, 4T1luc - Luciferase-transfected 4 T1 mouse mamma-carcinoma cells.

Study	Target	Dose delivered	Biodistribution		Efficacy
			whole-body	tissue-level	
Choi et al.	Neuro2A	2 to 3 % ID	→	↑	n.d.
Bartlett et al.		nt: 1.1 % ID/cm^3 t: 1.4 % ID/cm^3	→	n.d.	↑
Gu et al.	LNCaP	~ 0.2 to 1.8 %	↓	↑	n.d.
Kirpotin et al.	BT-474 or MCF-7	BT-474: nt: 7.3 % ID/g tissue t: 8.3 % ID/g tissue MCF-7: nt: 8.6 % ID/g tissue t: 7.2 % ID/g tissue	→	↑	n.d.
Bu et al.	MOC1	nt: ~$0.51x10^8$ TRE t: ~$2.1x10^8$ TRE	→	↑	n.d.
Zern et al.	Pulmonary vessels	n.d.	(↑)	↑	n.d.
Frigell et al.	Brain	nt: 0.0073 ID/g tissue t: 0.020 ID/g tissue	↓	(↑)	n.d.
Wang et al.	KB and MDA-MB-231 tumor	KB: nt: 3 % (4 h), 3 % (8 h) ID t: 5 % ID MDA-MB-231: nt: 2 % (4 h), 1 % (8 h) ID t: 3 % ID	(↑)	n.d.	n.d.
Ganesh et al.	$A549/A549^{DDP}$ (CD44 ↑) H69/H69AR (CD44 ↓) all NSCLC	t: 0.5–0.9 % ID nt: n.d.	(↑)	n.d.	↑ [127]
Akers et al.	4T1luc tumor	t: n.d. nt: n.d.	→	n.d.	n.d.

Table 2
Technology of particle platforms and ligand-receptor pairs employed for targeting. This table provides an overview about the type of particle systems investigated. We present the material of the particle technology used. In addition, we list the ligands used for functionalization with the according receptors addressed by them. We have compiled available data on these ligand-receptor pairs regarding their respective binding affinities, taking into account the method used for their determination. All relevant references are listed in the table. Abbreviations: ^{125}I - radioisotope of iodine, A10 RNA – 2′-fluoropyrimidine RNA aptamer, (a)PD-L1 - programmed cell death 1 ligand 1 (human antibodies), BLI - biolayer interferometry, CL4 - EGFR-binding nuclease-resistant RNA aptamer, cRGD(yK) - cyclic Arg-Gly-Asp peptide (D-Tyr-Lys-pentapeptide), [^{3}H]DAMGO - μ-opioid receptor ligand (structure: ^{3}H-Tyr-D-Ala-Gly-N-MePhe-Gly), DHM-^{3}H - ^{3}H-dihydromorphine, [^{3}H]DPDPE - δ-opioid ligand (structure: ^{3}H-D-Pen^2-D-Pen^5-enkephalin), EGFR - epidermal growth factor receptor, FP - fluorescence polarization, Glc - glucose, HER2 - human epidermal growth factor receptor 2, IC_{50} - half maximal inhibitory concentration, ICAM-1 - intercellular adhesion molecule 1, K_D - dissociation constant, K_i - inhibition constant, Leu-Enk - Leu-enkephalin, (rhu)(M)Ab - (recombinant human) (monoclonal) antibody, MOR/DOR - μ/δ-opioid receptor, n.d. - no data available, NAALADase - N-acetylated alpha-linked acidic dipeptidase, PAMAM - poly(amidoamine), PEG - polyethylene glycol, PEI - polyethylenimine, PFC - perfluorocarbon, PLGA-b-PEG - poly(ethylene glycol)-block-poly(D,L-lactic acid), PSMA - prostate-specific membrane antigen, PVPh - poly (4-vinylphen-ol), (si)RNA - (small interfering) ribonucleic acid, SPR - surface plasmon resonance, αvβ3 - integrin alpha V/integrin beta 3 receptor.

Study	Particle	Ligand	Receptor	affinity (technique)	Ref.
Choi et al. Bartlett et al.	PEGylated Au Gu complex	transferrin	transferrin receptor	K_{D1} = 1.1 nM, K_{D2} = 29 nM (SPR) K_{D1} < 0.1 nM* K_{D2} = 3.8 nM (SPR) K_D = 48 nM (^{125}I-lable)	[128–130]
Gu et al.	PLGA-b-PEG polymer	A10 RNA aptamer	PSMA	K_i = 11.9 nM (NAALADase activity)	[131]
Kirpotin et al.	PEGylated liposome	anti-HER2 MAb	HER2	rhuMAbHER2-Fab: K_D = 1.8 nM (SPR) anti-HER2 scFv F5: K_D = 160 nM (SPR)	[132–134]
Bu et al.	PAMAM dendrimers	aPD-L1	PD-L1	K_D = 0.96 nM (BLI), K_D = 0.38 nM (SPR)	[110]
Zern et al.	PVPh polymer	ICAM-1 Ab	ICAM-1	n.d.	–
Frigell et al.	Glc-coated Au	Leu-Enk	MOR/DOR	K_D = ~0.6 nM (DHM-^{3}H) IC_{50} μ = 1.8 nM ([^{3}H]DAMGO) IC_{50} δ = 0.6 nM ([^{3}H]DPDPE)	[135,136]
		Glycopep		n.d.	
Wang et al.	RNA	Folic acid	Folate receptor EGFR	K_D = 0.19 nM ([^{3}H]-folic acid)	[137,138]
		CL4 RNA aptamer		K_D = 10 nM (filter binding analysis)	
Ganesh et al.	PEI/PEG/siRNA	hyaluronic acid*	CD44	K_D = 21 μM (flow cytometry) K_D = 36.6 μM (SPR)	[139,140]
Akers et al.	PFC	cRGD	$\alpha_v\beta_3$	IC_{50} = 0.11 μM (FP) IC_{50} = 414/422/358 nM (^{125}I-echistatin) IC_{50} = 37 nM (^{125}I-c(RGDyK))	[141–145]

Chan [156] Drozdov et al. [157]. In brief summary the key factors known to date are opsonization of particle surface with biomolecules [158,159], undesired accumulation in the reticuloendothelial system (i.e., liver, spleen, lymph nodes) [103], access to tumor microenvironment (i.e., vessel evasion, endothelial crossing) [160], and navigating through complex tumor microenvironment (i.e., immune-cell interactions, extracellular matrix interactions, interstitial pressure) [161–165]. In this context, it is a pity that the studies of Wang et al. and Ganesh et al. do not contain any data on particle avidity and that also the degree of ligand functionalization was not varied. Thus, although these studies show that successful targeting is possible in tumor models, they do not allow a conclusion as to whether there is a correlation between avidity and biodistribution. A steep valency-dependent increase in avidity, however, has previously been demonstrated for folic acid-functionalized dendrimers (~4 nm) [65].

We would further like to point out a finding by Choi et al. that is important for the question about correlation between particle avidity and biodistribution. Besides the study by Zern et al. this is the only work in which a correlation between valency and avidity has been demonstrated. Although the authors find no influence of ligand functionalization in this case, an influence at the tissue level is noted. Concretely, the authors describe a threshold value for particle valence, above which a more favorable bio-distribution of the particle occurs. In our view, this observation raises the question about the 'reach' of avidity in biological systems. It must be discussed whether the attempt to directly transfer the avidity concept to the use case of particle distribution in a biological system may not be an oversimplification. Very valuable in this context is the study by Akers et al. which showed that a free ligand can even outperform a multivalently functionalized particle in terms of targeted delivery. Considering this the following points come to mind:

1) The unmodified transfer of the concept presupposes the assumption that the distribution of a particle between two tissues is determined exclusively or at least primarily by the process of binding per se. In other words, that there are no or only neglectable factors influencing distribution of the unbound particles other than undirected diffusion. As many studies on the troublesome road of nanoparticles to their target tissue already cited in this work have shown, this assumption must at least be considered bold.
2) An uncritical transfer further comes with a strong focus on ligand- and receptor-densities when attempting prediction of nanoparticle distribution. While this approach might be appropriate to derive meaningful binding parameters in experiments based on artificial or extracted membranes, it potentially oversimplifies the complexity of the surrounding encountered by the particle in an actual biological system. For instance, the cell membrane curvature is neglected, which we believe could be a crucial factor determining the availability of receptors for interaction with nanoparticles.

Previous work by our group indicates such importance of membrane

Table 3
Ligand-related nanoparticle properties and avidity-biodistribution correlation. This table gives an overview about the nanoparticle properties size, valency, and ligand density. We have also included data on nanoparticle avidity where it was investigated. Finally, we list our conclusions on presence and nature of correlation between nanoparticle valency (N) and avidity (K) as well as between valency and whole-body (w-b) and tissue-level (t-l) biodistribution. Abbreviations:? - no conclusion possible based on present data, E - enkephalin-functionalization, G - glycopep-functionalization, (Mut)Apt - (mutated i.e., non-functional) aptamer, N.A. - not applicable, n.d. - no data available.

Study	size [nm]	*N*	ligand density	particle avidity	valency *N* dependence?	
					K	biodistribution
Choi et al.	74.9 77.7 81.3 87.5	control 2.1 17.5 144.3	0 nm^{-3} 1.1 x10^{-4} nm^{-3} 8.4 x10^{-4} nm^{-3} 6.0 x10^{-3} nm^{-3}	n.d. n.d. 1.06 nM 0.13 nM	yes	w-b.: no t-l.:threshold for particle uptake in target cells
Bartlett et al.	~80 to 125	n.d.	n.d	n.d.	?	?
Gu et al.	160	n.d.	10 % MutApt 0 % Apt 1 % Apt 5 % Apt 10 % Apt	n.d.	?	w-b.: no t-l.:tumor accumulation increases with % Apt up to 5 % Apt then decreases.
Kirpotin et al.	~90 to 110	> 20	~5.3 x10^{-4} nm^{-3} to 7.9 x10^{-4} nm^{-3}	n.d.	?	?
Bu et al.	~25 to 35	3.7	~9.6 x10^{-4} nm^{-3} to 1.9 x10^{-3} nm^{-3}	targeted: 85/66 fM blank: 0.96/ 0.38 nM	?	w-b.: no t-l.:ligand induces significant increase in dose delivered to tumor.
Zern et al.	187 183 186 192 198	blank 5 50 100 200	0 nm^{-3} 1.1 x10^{-4} nm^{-3} 8.4 x10^{-4} nm^{-3} 6.0 x10^{-3} nm^{-3} 6.0 x10^{-3} nm^{-3}	n.d. n.d. 1.0 x10^{10} nm^3 n.d. 1.2 x10^{11} nm^3	yes	w-b.:particle dose in liver appears to decrease with increasing *N*. t-l.:Dose accumulated in lungs increases with increasing *N*.
Frigell et al.	2.4 2.1 2.7 2.2 3.2	blank 13 E 10 E 6 G 15 G	0 nm^{-3} 0.94 nm^{-3} 0.44 nm^{-3} 0.39 nm^{-3} 0.47 nm^{-3}	n.d.	?	w-b.:Partially, ligands increase accumulation in off-target organs. t-l.:One ligand-linker pairing induced higher dose in target organ.
Wang et al.	6.0[1]/ 14.8[2]	n.d.	n.d.	n.d.	?	?
Ganesh et al.	200/ 90 to 100	N.A.	N.A.	N.A.	?	?
Akers et al.	250	n.d.	n.d.	n.d.	?	?

nanomorphology. A significant decrease in avidity was observed for a model particle system after inhibition of clathrin-coated pits (CCPs) as typical nanostructures in the membrane [96]. We also observed that biomolecules more abundant in tumors, which might have a comparable effect on CCPs, unfavorably influence the distribution of particles between target and off-target cells [166].

Overall, the present review identifies an urgent need for systematic fundamental research. We have outlined two possible approaches for a systematic proceeding to stimulate research that could lead to a better understanding of nano-bio-interactions (Fig. 9A) and the correlation of avidity and biodistribution (Fig. 9B).

Lastly, we intend to point out some issues that in our view prevent a better understanding of nanoparticle distribution in biological systems. It is striking that, to our knowledge, there are no studies available that investigate the influence of dose titration on nanoparticle biodistribution. In general, a rationale for the administered dose is rarely given. It is understandable and appropriate that application-oriented studies focus on the effect of a nanotherapeutic system. However, we also consider fundamental research necessary that investigates the relationship between dose and biodistribution. Especially since in vitro experiments conducted by our group have shown that target cell specificity of ligand-functionalized nanoparticles strongly depends on the dose applied [166]. One methodological problem is the occasional lack of non-ligand-functionalized control particles. The lack of such controls makes it difficult to evaluate the observed biodistribution, as the influence of ligand functionalization cannot be assessed.

Finally, the question arises as to whether tissue-specific delivery is the optimal application for high-avidity nanoparticles. Results from our group show that they are also suitable for making otherwise inaccessible tissues accessible for their payload. In this context, we were successful in developing particles for transport into the glomerular mesangial cells [167,168], the retina [169,170] as well as specific immune cells [171].

7. Conclusion

The overview of data available on the correlation of nanoparticle avidity and biodistribution provided in this work revealed that the matter is strongly under-researched. After a thorough review of the available literature, we cannot draw a definitive conclusion whether an increasing particle avidity will lead to increased particle accumulation at the desired target site. Since this observation stands in contradiction with the theoretical fundamentals of avidity, this in turn allows for four conclusions: (A) The particle avidity is influenced by to date unknown factors that counteract its expected positive effect on biodistribution, (B) all systems studied so far in literature exhibit extremely high entropic penalties that prevent the formation of ligand-receptor interactions, (C) The concept of avidity is in fact not applicable to the case of particle distribution in a biological system, and (D) the data collected so far are not sufficient to recognize any correlation that may exist. In summary our work has revealed a significant lack of systematic studies on this matter. In this context, we understand a systematic study as an investigation of the biodistribution of a series of particles with varying quantified avidity (e.g., using SPR) in a biological model organism with a subsequent quantitative investigation of the presence and if given the nature of the correlation

With these approaches, our work has the potential to stimulate further research that may lead to a better understanding of the interplay between avidity and biodistribution. Further insights in this field could in turn contribute to the development of improved targeted delivery systems. Basis of the present work was the research need arising from point (A) to identify factors influencing the avidity of particles when interacting with their target cells.

CRediT authorship contribution statement

Oliver Zimmer: Conceptualization, Formal analysis, Investigation, Methodology, Visualization, Writing – original draft, Writing – review & editing. **Achim Goepferich:** Conceptualization, Funding acquisition, Project administration, Resources, Supervision, Writing – original draft, Writing – review & editing.

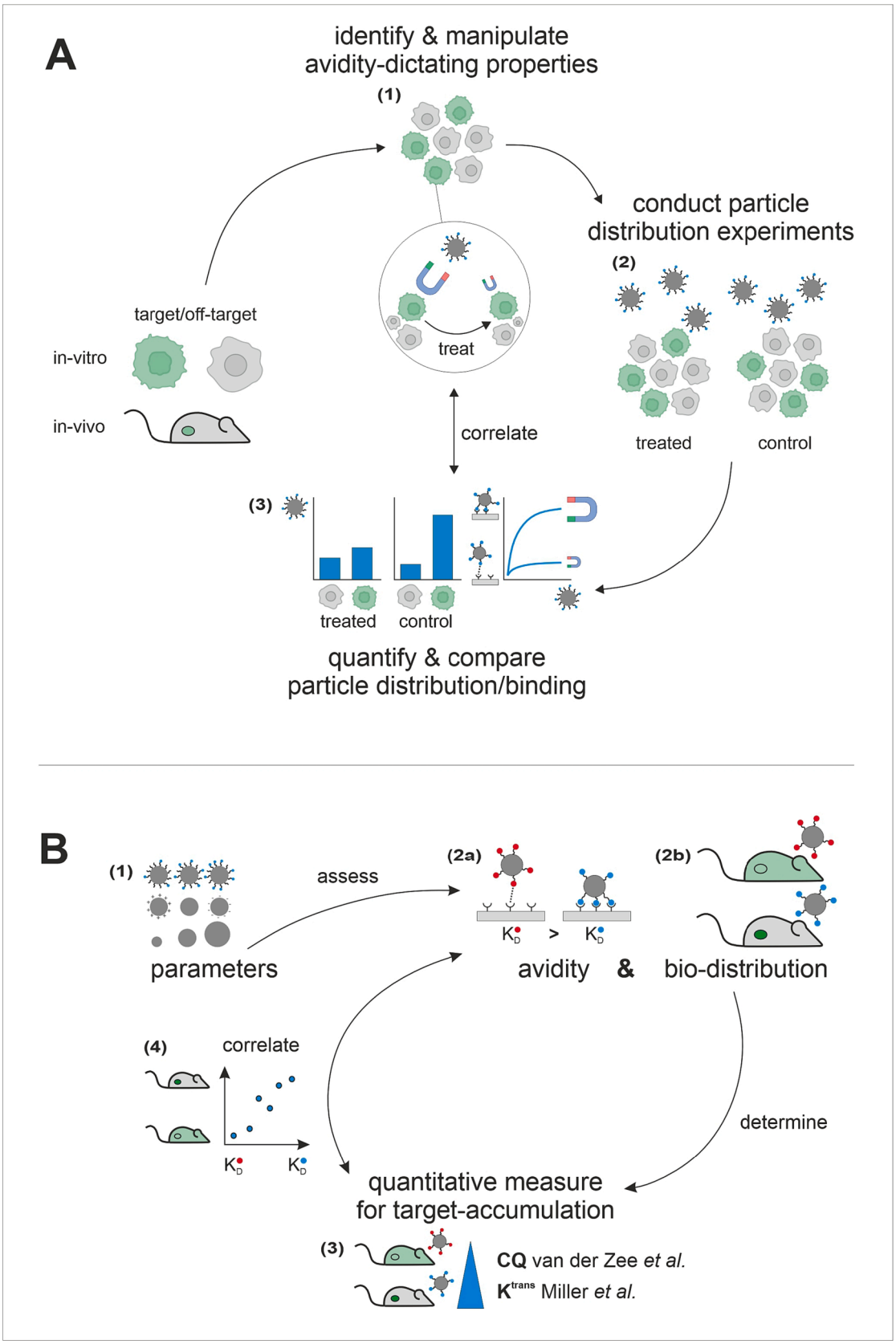

(caption on next page)

Fig. 9. Approaches for systematic investigation of nano-bio-interactions and avidity-biodistribution studies. In these schemes we outline principal study proceedings suitable to (A) identify and characterize biological properties affecting nanoparticle avidity and (B) to systematically investigate the correlation of nanoparticle avidity and biodistribution. (A) A more complete understanding of biological parameters affecting nanoparticle-cell interactions is key to increase predictability of particle biodistribution. For this, a systematic proceeding is outlined above, which in brief suggests to (1) hypothesize parameters to investigate and to identify tools enabling controlled manipulation of these properties, (2) to conduct particle binding or distribution assays, where possible in a cellular or even in an in vivo setting, and (3) to quantify and compare binding or distribution data for a series of parameter states. Optimally, the correlation of parameter state and binding/distribution data should be studied to identify a model describing their interaction. This could allow not only to identify the presence of a correlation but also to understand its precise nature. (B) One circumstance that complicates the assessment of avidity-biodistribution correlation is that there have been only few studies with a dedicated focus on the matter. Most of the knowledge available today on this subject must be gathered from individual publications, each of which often contains only incomplete sets of information on the relationship in question. We outline here a blueprint for an approach to systematically investigate the relationship between avidity and biodistribution. In brief, (1) the particle parameters to be studied should be varied individually and in a controlled manner. In this way, a design space for the studied particle can be covered. (2) Both avidity and bio-distribution should be determined for each individual particle. Finally, (3) a correlation analysis should be performed to investigate the relationship between avidity and bio-distribution. In this step, it is preferable to use quantitative measures for the degree of accumulation [146], to in turn allow for a subsequent quantitative assessment of correlation. Applicable parameters were presented in the literature by van der Zee et al. [172] and Miller et al. [173].

Conflicts of Interest

The authors declare that they have no known competing financial interests or personal relationships that could have appeared to influence the work reported in this paper.

Data availability

Data will be made available on request.

Acknowledgments

This work was supported by German Research Foundation (Deutsche Forschungsgemeinschaft, DFG) grant GO 565/20-1.

References

[1] J.K. Mills, D. Needham, Targeted drug delivery, Expert Opin. Ther. Pat. 9 (1999) 1499–1513.
[2] P. Kumari, B. Ghosh, S. Biswas, Nanocarriers for cancer-targeted drug delivery, J. Drug Target. 24 (2016) 179–191.
[3] A.I. Freeman, E. Mayhew, Targeted drug delivery, Cancer 58 (1986) 573–583.
[4] S. Sur, A. Rathore, V. Dave, K.R. Reddy, R.S. Chouhan, V. Sadhu, Recent developments in functionalized polymer nanoparticles for efficient drug delivery system, Nano-Structures & Nano-Objects 20 (2019) 100397.
[5] M. Srinivasarao, P.S. Low, Ligand-targeted drug delivery, Chem. Rev. 117 (2017) 12133–12164.
[6] S.-W. Choi, W.-S. Kim, J.-H. Kim, Surface modification of functional nanoparticles for controlled drug delivery, J. Dispers. Sci. Technol. 24 (2003) 475–487.
[7] N.H. Abd Ellah, S.A. Abouelmagd, Surface functionalization of polymeric nanoparticles for tumor drug delivery: approaches and challenges, Expert Opinion on Drug Delivery 14 (2017) 201–214.
[8] M.J. Akhtar, M. Ahamed, H.A. Alhadlaq, S.A. Alrokayan, S. Kumar, Targeted anticancer therapy: overexpressed receptors and nanotechnology, Clinica Chimica Acta; International Journal of Clinical Chemistry 436 (2014) 78–92.
[9] M. Walter, F. Baumann, K. Schorr, A. Goepferich, Ectoenzymes as promising cell identification structures for the high avidity targeting of polymeric nanoparticles, Int. J. Pharm. (2023) 123453.
[10] S. Xu, B.Z. Olenyuk, C.T. Okamoto, S.F. Hamm-Alvarez, Targeting receptor-mediated endocytotic pathways with nanoparticles: rationale and advances, Adv. Drug Deliv. Rev. 65 (2013) 121–138.
[11] G.T. Tietjen, L.G. Bracaglia, W.M. Saltzman, J.S. Pober, Focus on fundamentals: achieving effective nanoparticle targeting, Trends Mol. Med. 24 (2018) 598–606.
[12] Z.G. Chen, Small-molecule delivery by nanoparticles for anticancer therapy, Trends Mol. Med. 16 (2010) 594–602.
[13] A. Lalatsa, A.G. Schatzlein, I.F. Uchegbu, Strategies to deliver peptide drugs to the brain, Mol. Pharm. 11 (2014) 1081–1093.
[14] S.-J. Cao, S. Xu, H.-M. Wang, Y. Ling, J. Dong, R.-D. Xia, X.-H. Sun, Nanoparticles: Oral delivery for protein and peptide drugs, AAPS PharmSciTech 20 (2019) 190.
[15] A. Zeb, I. Rana, H.-I. Choi, C.-H. Lee, S.-W. Baek, C.-W. Lim, N. Khan, S.T. Arif, N. U. Sahar, A.M. Alvi, F.A. Shah, F.U. Din, O.-N. Bae, J.-S. Park, J.-K. Kim, Potential and applications of nanocarriers for efficient delivery of biopharmaceuticals, Pharmaceutics 12 (2020).
[16] S. Mitragotri, P.A. Burke, R. Langer, Overcoming the challenges in administering biopharmaceuticals: formulation and delivery strategies, Nat. Rev. Drug Discov. 13 (2014) 655–672.
[17] Y. Xiao, K. Shi, Y. Qu, B. Chu, Z. Qian, Engineering nanoparticles for targeted delivery of nucleic acid therapeutics in tumor, Molecular Therapy. Methods & Clinical Development 12 (2019) 1–18.
[18] A. Amani, M.R. Alizadeh, H. Yaghoubi, M. Nohtani, Novel multi-targeted nanoparticles for targeted co-delivery of nucleic acid and chemotherapeutic agents to breast cancer tissues, Materials science & engineering: C, Materials for Biological Applications 118 (2021) 111494.
[19] J. Karlsson, K.M. Luly, S.Y. Tzeng, J.J. Green, Nanoparticle designs for delivery of nucleic acid therapeutics as brain cancer therapies, Adv. Drug Deliv. Rev. 179 (2021) 113999.
[20] H.J. Vaughan, J.J. Green, S.Y. Tzeng, Cancer-targeting nanoparticles for combinatorial nucleic acid delivery, advanced materials, Advanced materials (Deerfield Beach, Fla.) 32 (2020) e1901081.
[21] H.I. Labouta, R. Langer, P.R. Cullis, O.M. Merkel, M.R. Prausnitz, Y. Gomaa, S. S. Nogueira, T. Kumeria, Role of drug delivery technologies in the success of COVID-19 vaccines: a perspective, Drug Deliv. Transl. Res. 12 (2022) 2581–2588.
[22] F. Meng, J. Wang, Q. Ping, Y. Yeo, Quantitative assessment of nanoparticle biodistribution by fluorescence imaging, revisited, ACS Nano 12 (2018) 6458–6468.
[23] I.H.C. Miedema, G.J.C. Zwezerijnen, M.C. Huisman, E. Doeleman, R.H. J. Mathijssen, T. Lammers, Q. Hu, G.A.M.S. van Dongen, C.J.F. Rijcken, D. J. Vugts, C.W. Menke-van der Houven van Oordt, PET-CT imaging of polymeric nanoparticle tumor accumulation in patients, Advanced materials (Deerfield Beach, Fla.) 34 (2022) e2201043.
[24] S.J. Blocker, A.F. Shields, Imaging of nanoparticle distribution to assess treatments that Alter delivery, Mol. Imag. Biol. 20 (2018) 340–351.
[25] O. Kochebina, A. Halty, J. Taleb, D. Kryza, M. Janier, A.B. Sadr, T. Baudier, S. Rit, D. Sarrut, In vivo gadolinium nanoparticle quantification with SPECT/CT, EJNMMI Physics 6 (2019) 9.
[26] M. Torrice, Does nanomedicine have a delivery problem? ACS Cent. Sci. 2 (2016) 434–437.
[27] R. Cai, C. Chen, The crown and the scepter: roles of the protein Corona in nanomedicine, Advanced materials (Deerfield Beach, Fla.) 31 (2019) e1805740.
[28] C. Corbo, R. Molinaro, A. Parodi, N.E. Toledano Furman, F. Salvatore, E. Tasciotti, The impact of nanoparticle protein corona on cytotoxicity, immunotoxicity and target drug delivery, Nanomedicine (London, England) 11 (2016) 81–100.
[29] W. Xiao, H. Gao, The impact of protein corona on the behavior and targeting capability of nanoparticle-based delivery system, Int. J. Pharm. 552 (2018) 328–339.
[30] M.A. Dobrovolskaia, P. Aggarwal, J.B. Hall, S.E. McNeil, Preclinical studies to understand nanoparticle interaction with the immune system and its potential effects on nanoparticle biodistribution, Mol. Pharm. 5 (2008) 487–495.
[31] S.M. Moghimi, Chemical camouflage of nanospheres with a poorly reactive surface: towards development of stealth and target-specific nanocarriers, BBA 1590 (2002) 131–139.
[32] D. van Haute, J.M. Berlin, Challenges in realizing selectivity for nanoparticle biodistribution and clearance: lessons from gold nanoparticles, Ther. Deliv. 8 (2017) 763–774.
[33] M. Cataldi, C. Vigliotti, T. Mosca, M. Cammarota, D. Capone, Emerging role of the spleen in the pharmacokinetics of monoclonal antibodies, nanoparticles and exosomes, Int. J. Mol. Sci. 18 (2017).
[34] W. Xu, M. Xu, Y. Xiao, L. Yu, H. Xie, X. Jiang, M. Chen, H. Gao, L. Wang, Changes in target ability of nanoparticles due to protein corona composition and disease state, Asian J. Pharm. Sci. 17 (2022) 401–411.
[35] A. Salvati, A.S. Pitek, M.P. Monopoli, K. Prapainop, F.B. Bombelli, D.R. Hristov, P. M. Kelly, C. Åberg, E. Mahon, K.A. Dawson, Transferrin-functionalized nanoparticles lose their targeting capabilities when a biomolecule corona adsorbs on the surface, Nat. Nanotechnol. 8 (2013) 137–143.
[36] T. Malachowski, A. Hassel, Engineering nanoparticles to overcome immunological barriers for enhanced drug delivery, Engineered Regeneration 1 (2020) 35–50.
[37] B.S. Zolnik, A. González-Fernández, N. Sadrieh, M.A. Dobrovolskaia, Nanoparticles and the immune system, Endocrinology 151 (2010) 458–465.
[38] J.J. Milligan, S. Saha, A nanoparticle's journey to the tumor: strategies to overcome first-pass metabolism and their limitations, Cancers 14 (2022).
[39] J.L. Cuellar-Camacho, S. Bhatia, V. Reiter-Scherer, D. Lauster, S. Liese, J.P. Rabe, A. Herrmann, R. Haag, Quantification of multivalent interactions between sialic acid and influenza a virus spike proteins by single-molecule force spectroscopy, J. Am. Chem. Soc. 142 (2020) 12181–12192.

[40] D. Di Iorio, M.L. Verheijden, E. van der Vries, P. Jonkheijm, J. Huskens, Weak multivalent binding of influenza hemagglutinin nanoparticles at a sialoglycan-functionalized supported lipid bilayer, ACS Nano 13 (2019) 3413–3423.
[41] H. Jung, A.D. Robison, P.S. Cremer, Multivalent ligand-receptor binding on supported lipid bilayers, J. Struct. Biol. 168 (2009) 90–94.
[42] J.E. Silpe, M. Sumit, T.P. Thomas, B. Huang, A. Kotlyar, M.A. van Dongen, M. M. Banaszak Holl, B.G. Orr, S.K. Choi, Avidity modulation of folate-targeted multivalent dendrimers for evaluating biophysical models of cancer targeting nanoparticles, ACS Chem. Biol. 8 (2013) 2063–2071.
[43] D. Lauster, M. Glanz, M. Bardua, K. Ludwig, M. Hellmund, U. Hoffmann, A. Hamann, C. Böttcher, R. Haag, C.P.R. Hackenberger, A. Herrmann, Multivalent Peptide-Nanoparticle Conjugates for Influenza-Virus Inhibition, Angewandte Chemie (International ed. in English) 56 (2017) 5931–5936.
[44] D. Peterhoff, S. Thalhauser, P. Neckermann, C. Barbey, K. Straub, J. Nazet, R. Merkl, G. Laengst, M. Breunig, R. Wagner, Multivalent Display of Engineered HIV-1 Envelope Trimers on Silica Nanoparticles for Targeting and in Vitro Activation of Germline VRC01 B Cells, European Journal of Pharmaceutics and Biopharmaceutics 181 (2022) 88–101.
[45] D.E. Owens, N.A. Peppas, Opsonization, biodistribution, and pharmacokinetics of polymeric nanoparticles, Int. J. Pharm. 307 (2006) 93–102.
[46] S. Erlendsson, K. Teilum, Binding revisited-avidity in cellular function and signaling, Front. Mol. Biosci. 7 (2020) 615565.
[47] M.I. Page, W.P. Jencks, Entropic contributions to rate accelerations in enzymic and intramolecular reactions and the chelate effect, PNAS 68 (1971) 1678–1683.
[48] W.P. Jencks, On the attribution and additivity of binding energies, PNAS 78 (1981) 4046–4050.
[49] P.I. Kitov, D.R. Bundle, On the nature of the multivalency effect: a thermodynamic model, J. Am. Chem. Soc. 125 (2003) 16271–16284.
[50] V.M. Krishnamurthy, L.A. Estroff, G.M. Whitesides, Multivalency in ligand design, in: W. Jahnke, D.A. Erlanson (Eds.), Fragment-Based Approaches in Drug Discovery, Wiley, 2006, pp. 11–53.
[51] C.A. Hunter, H.L. Anderson, What is cooperativity? Angewandte Chemie (International ed. in English) 48 (2009) 7488–7499.
[52] C.H. Reynolds, M.K. Holloway, Thermodynamics of ligand binding and efficiency, ACS Med. Chem. Lett. 2 (2011) 433–437.
[53] M.K. Gilson, T. Liu, M. Baitaluk, G. Nicola, L. Hwang, J. Chong, BindingDB in 2015: A public database for medicinal chemistry, computational chemistry and systems pharmacology, Nucleic Acids Res. 44 (2016) D1045–D1053.
[54] T. Liu, Y. Lin, X. Wen, R.N. Jorissen, M.K. Gilson, BindingDB: a web-accessible database of experimentally determined protein-ligand binding affinities, Nucleic Acids Res. 35 (2007) D198–D201.
[55] T.S.G. Olsson, M.A. Williams, W.R. Pitt, J.E. Ladbury, The thermodynamics of protein-ligand interaction and solvation: insights for ligand design, J. Mol. Biol. 384 (2008) 1002–1017.
[56] G. Schwarzenbach, Der chelateffekt, Helv. Chim. Acta 35 (1952) 2344–2359.
[57] A.V. Finkelstein, J. Janin, The price of lost freedom: entropy of bimolecular complex formation, Protein Eng. 3 (1989) 1–3.
[58] S. Maslanka Figueroa, D. Fleischmann, S. Beck, A. Goepferich, The effect of ligand mobility on the cellular interaction of multivalent nanoparticles, Macromol. Biosci. 20 (2020) e1900427.
[59] M. de Amici, C. Dallanoce, U. Holzgrabe, C. Tränkle, K. Mohr, Allosteric ligands for G protein-coupled receptors: a novel strategy with attractive therapeutic opportunities, Med. Res. Rev. 30 (2010) 463–549.
[60] F.J. Martinez-Veracoechea, D. Frenkel, Designing super selectivity in multivalent nano-particle binding, PNAS 108 (2011) 10963–10968.
[61] P.A. Borea, K. Varani, S. Gessi, P. Gilli, A. Dalpiaz, Receptor binding thermodynamics as a tool for linking drug efficacy and affinity, Farmaco (societa Chimica Italiana 1989) 53 (1998) 249–254.
[62] I. Nakase, N. Ueno, M. Katayama, K. Noguchi, T. Takatani-Nakase, N. B. Kobayashi, T. Yoshida, I. Fujii, S. Futaki, Receptor clustering and activation by multivalent interaction through recognition peptides presented on exosomes, Chem. Commun. (Camb.) 53 (2016) 317–320.
[63] Y.-F. Huang, H. Liu, X. Xiong, Y. Chen, W. Tan, Nanoparticle-mediated IgE-receptor aggregation and signaling in RBL mast cells, J. Am. Chem. Soc. 131 (2009) 17328–17334.
[64] M.B. Deci, M. Liu, Q.T. Dinh, J. Nguyen, Precision engineering of targeted nanocarriers, Wiley Interdiscip. Rev. Nanomed. Nanobiotechnol. 10 (2018) e1511.
[65] S. Hong, P.R. Leroueil, I.J. Majoros, B.G. Orr, J.R. Baker, M.M. Banaszak Holl, The binding avidity of a nanoparticle-based multivalent targeted drug delivery platform, Chem. Biol. 14 (2007) 107–115.
[66] C. He, Y. Hu, L. Yin, C. Tang, C. Yin, Effects of particle size and surface charge on cellular uptake and biodistribution of polymeric nanoparticles, Biomaterials 31 (2010) 3657–3666.
[67] S. Hirn, M. Semmler-Behnke, C. Schleh, A. Wenk, J. Lipka, M. Schäffler, S. Takenaka, W. Möller, G. Schmid, U. Simon, W.G. Kreyling, Particle Size-Dependent and Surface Charge-Dependent Biodistribution of Gold Nanoparticles after Intravenous Administration, European Journal of Pharmaceutics and Biopharmaceutics 77 (2011) 407–416.
[68] D.L. Jasinski, H. Li, P. Guo, The effect of size and shape of RNA nanoparticles on biodistribution, molecular therapy the journal of the american society of, Gene Ther. 26 (2018) 784–792.
[69] G. Sonavane, K. Tomoda, K. Makino, Biodistribution of colloidal gold nanoparticles after intravenous administration: effect of particle size, Colloids and surfaces. B, Biointerfaces 66 (2008) 274–280.
[70] P. Decuzzi, B. Godin, T. Tanaka, S.-Y. Lee, C. Chiappini, X. Liu, M. Ferrari, Size and shape effects in the biodistribution of intravascularly injected particles, J. Control. Release 141 (2010) 320–327.
[71] G. Zhang, Z. Yang, W. Lu, R. Zhang, Q. Huang, M. Tian, L. Li, D. Liang, C. Li, Influence of anchoring ligands and particle size on the colloidal stability and in vivo biodistribution of polyethylene glycol-coated gold nanoparticles in tumor-xenografted mice, Biomaterials 30 (2009) 1928–1936.
[72] S.A. Kulkarni, S.-S. Feng, Effects of particle size and surface modification on cellular uptake and biodistribution of polymeric nanoparticles for drug delivery, Pharm. Res. 30 (2013) 2512–2522.
[73] F. Alexis, E. Pridgen, L.K. Molnar, O.C. Farokhzad, Factors affecting the clearance and biodistribution of polymeric nanoparticles, Mol. Pharm. 5 (2008) 505–515.
[74] J.M. Caster, S.K. Yu, A.N. Patel, N.J. Newman, Z.J. Lee, S.B. Warner, K.T. Wagner, K.C. Roche, X. Tian, Y. Min, A.Z. Wang, Effect of particle size on the biodistribution, toxicity, and efficacy of drug-loaded polymeric nanoparticles in chemoradiotherapy, Nanomed. Nanotechnol. Biol. Med. 13 (2017) 1673–1683.
[75] S. Kaga, N.P. Truong, L. Esser, D. Senyschyn, A. Sanyal, R. Sanyal, J.F. Quinn, T. P. Davis, L.M. Kaminskas, M.R. Whittaker, Influence of size and shape on the biodistribution of nanoparticles prepared by polymerization-induced self-assembly, Biomacromolecules 18 (2017) 3963–3970.
[76] K. Xiao, Y. Li, J. Luo, J.S. Lee, W. Xiao, A.M. Gonik, R.G. Agarwal, K.S. Lam, The effect of surface charge on in vivo biodistribution of PEG-oligocholic acid based micellar nanoparticles, Biomaterials 32 (2011) 3435–3446.
[77] L. Maurizi, A.-L. Papa, L. Dumont, F. Bouyer, P. Walker, D. Vandroux, N. Millot, Influence of surface charge and polymer coating on internalization and biodistribution of polyethylene glycol-modified iron oxide nanoparticles, J. Biomed. Nanotechnol. 11 (2015) 126–136.
[78] S.G. Elci, Y. Jiang, B. Yan, S.T. Kim, K. Saha, D.F. Moyano, G. Yesilbag Tonga, L. C. Jackson, V.M. Rotello, R.W. Vachet, Surface charge controls the suborgan biodistributions of gold nanoparticles, ACS Nano 10 (2016) 5536–5542.
[79] X. Huang, L. Li, T. Liu, N. Hao, H. Liu, D. Chen, F. Tang, The shape effect of mesoporous silica nanoparticles on biodistribution, clearance, and biocompatibility in vivo, ACS Nano 5 (2011) 5390–5399.
[80] L. Li, T. Liu, C. Fu, L. Tan, X. Meng, H. Liu, Biodistribution, excretion, and toxicity of mesoporous silica nanoparticles after oral administration depend on their shape, Nanomed. Nanotechnol. Biol. Med. 11 (2015) 1915–1924.
[81] D. Shao, M.-M. Lu, Y.-W. Zhao, F. Zhang, Y.-F. Tan, X. Zheng, Y. Pan, X.-A. Xiao, Z. Wang, W.-F. Dong, J. Li, L. Chen, The shape effect of magnetic mesoporous silica nanoparticles on endocytosis, biocompatibility and biodistribution, Acta Biomater. 49 (2017) 531–540.
[82] S. Shukla, F.J. Eber, A.S. Nagarajan, N.A. DiFranco, N. Schmidt, A.M. Wen, S. Eiben, R.M. Twyman, C. Wege, N.F. Steinmetz, The impact of aspect ratio on the biodistribution and tumor homing of rigid soft-matter nanorods, Adv. Healthc. Mater. 4 (2015) 874–882.
[83] T. Harayama, H. Riezman, Understanding the diversity of membrane lipid composition, Nat. Rev. Mol. Cell Biol. 19 (2018) 281–296.
[84] E. Sezgin, I. Levental, S. Mayor, C. Eggeling, The mystery of membrane organization: composition, regulation and roles of lipid rafts, Nat. Rev. Mol. Cell Biol. 18 (2017) 361–374.
[85] A. Gray, E. Abbena, S. Salamon, Modern differential geometry curves and surfaces with mathematica by Alfred gray, Elsa abbena and Simon salamon, 3rd ed., Chapman & Hall/CRC, Boca Raton, 2006.
[86] E.E. Kooijman, V. Chupin, N.L. Fuller, M.M. Kozlov, B. de Kruijff, K.N.J. Burger, P.R. Rand, Spontaneous curvature of phosphatidic acid and lysophosphatidic acid, Biochemistry 44 (2005) 2097–2102.
[87] M.K. Dymond, Lipid monolayer spontaneous curvatures: a collection of published values, Chem. Phys. Lipids 239 (2021) 105117.
[88] J. Zimmerberg, M.M. Kozlov, How proteins produce cellular membrane curvature, Nat. Rev. Mol. Cell Biol. 7 (2006) 9–19.
[89] J. Agudo-Canalejo, R. Lipowsky, Adhesive nanoparticles as local probes of membrane curvature, Nano Lett. 15 (2015) 7168–7173.
[90] J. Agudo-Canalejo, R. Lipowsky, Uniform and janus-like nanoparticles in contact with vesicles: energy landscapes and curvature-induced forces, Soft Matter 13 (2017) 2155–2173.
[91] Q. Yu, S. Othman, S. Dasgupta, T. Auth, G. Gompper, Nanoparticle wrapping at small non-spherical vesicles: curvatures at play, Nanoscale 10 (2018) 6445–6458.
[92] M. Deserno, T. Bickel, Wrapping of a spherical colloid by a fluid membrane, Europhys. Lett. 62 (2003) 767–774.
[93] A.H. Bahrami, R. Lipowsky, T.R. Weikl, The role of membrane curvature for the wrapping of nanoparticles, Soft Matter 12 (2016) 581–587.
[94] K.A. Sochacki, B.L. Heine, G.J. Haber, J.R. Jimah, B. Prasai, M.A. Alfonzo-Méndez, A.D. Roberts, A. Somasundaram, J.E. Hinshaw, J.W. Taraska, The structure and spontaneous curvature of clathrin lattices at the plasma membrane, Dev. Cell 56 (2021) 1131–1146.e3.
[95] A.A. Yetisgin, S. Cetinel, M. Zuvin, A. Kosar, O. Kutlu, Therapeutic Nanoparticles and Their Targeted Delivery Applications, Molecules (Basel, Switzerland) 25 (2020).
[96] O. Zimmer, A. Goepferich, How clathrin-coated pits control nanoparticle avidity for cells, Nanoscale Horiz. 8 (2023) 256–269.
[97] C.H.J. Choi, C.A. Alabi, P. Webster, M.E. Davis, Mechanism of active targeting in solid tumors with transferrin-containing gold nanoparticles, PNAS 107 (2010) 1235–1240.
[98] N.J. Butcher, G.M. Mortimer, R.F. Minchin, Drug delivery: unravelling the stealth effect, Nat. Nanotechnol. 11 (2016) 310–311.
[99] S.-D. Li, L. Huang, Stealth nanoparticles: high density but sheddable PEG is a key for tumor targeting, J. Control. Release 145 (2010) 178–181.

[100] S. Zalba, T.L.M. ten Hagen, C. Burgui, M.J. Garrido, Stealth nanoparticles in oncology: facing the PEG dilemma, J. Control. Release 351 (2022) 22–36.
[101] F. Gu, L. Zhang, B.A. Teply, N. Mann, A. Wang, A.F. Radovic-Moreno, R. Langer, O.C. Farokhzad, Precise engineering of targeted nanoparticles by using self-assembled biointegrated block copolymers, PNAS 105 (2008) 2586–2591.
[102] N. Hoshyar, S. Gray, H. Han, G. Bao, The effect of nanoparticle size on in vivo pharmacokinetics and cellular interaction, Nanomedicine (Lond.) 11 (2016) 673–692.
[103] Y.-N. Zhang, W. Poon, A.J. Tavares, I.D. McGilvray, W.C.W. Chan, Nanoparticle-liver interactions: cellular uptake and hepatobiliary elimination, J. Control. Release 240 (2016) 332–348.
[104] W. Ngo, S. Ahmed, C. Blackadar, B. Bussin, Q. Ji, S.M. Mladjenovic, Z. Sepahi, W. C.W. Chan, Why nanoparticles prefer liver macrophage cell uptake in vivo, Adv. Drug Deliv. Rev. 185 (2022) 114238.
[105] J.W. Park, K. Hong, D.B. Kirpotin, G. Colbern, R. Shalaby, J. Baselga, Y. Shao, U. B. Nielsen, J.D. Marks, D. Moore, D. Papahadjopoulos, C.C. Benz, Anti-HER2 immunoliposomes: enhanced efficacy attributable to targeted delivery, clinical cancer research an official journal of the american association for, Cancer Res. 8 (2002) 1172–1181.
[106] D.B. Kirpotin, D.C. Drummond, Y. Shao, M.R. Shalaby, K. Hong, U.B. Nielsen, J. D. Marks, C.C. Benz, J.W. Park, Antibody targeting of long-circulating lipidic nanoparticles does not increase tumor localization but does increase internalization in animal models, Cancer Res. 66 (2006) 6732–6740.
[107] D.W. Bartlett, M.E. Davis, Physicochemical and biological characterization of targeted, nucleic acid-containing nanoparticles, Bioconjug. Chem. 18 (2007) 456–468.
[108] D.W. Bartlett, H. Su, I.J. Hildebrandt, W.A. Weber, M.E. Davis, Impact of tumor-specific targeting on the biodistribution and efficacy of siRNA nanoparticles measured by multimodality in vivo imaging, Proceedings of the National Academy of Sciences of the United States of America 104 (2007) 15549–15554.
[109] J. Wang, J. Min, S.A. Eghtesadi, R.S. Kane, A. Chilkoti, Quantitative study of the interaction of multivalent ligand-modified nanoparticles with breast cancer cells with tunable receptor density, ACS Nano 14 (2020) 372–383.
[110] J. Bu, A. Nair, M. Iida, W.-J. Jeong, M.J. Poellmann, K. Mudd, L.J. Kubiatowicz, E. W. Liu, D.L. Wheeler, S. Hong, An avidity-based PD-L1 antagonist using nanoparticle-antibody conjugates for enhanced immunotherapy, Nano Lett. 20 (2020) 4901–4909.
[111] G.M. Thurber, K. Dane Wittrup, A mechanistic compartmental model for total antibody uptake in tumors, J. Theor. Biol. 314 (2012) 57–68.
[112] G.P. Adams, R. Schier, A.M. McCall, H.H. Simmons, E.M. Horak, R.K. Alpaugh, J. D. Marks, L.M. Weiner, High affinity restricts the localization and tumor penetration of single-chain fv antibody molecules, Cancer Res. 61 (2001) 4750–4755.
[113] M.M. Schmidt, K.D. Wittrup, A modeling analysis of the effects of molecular size and binding affinity on tumor targeting, Mol. Cancer Ther. 8 (2009) 2861–2871.
[114] B.J. Zern, A.-M. Chacko, J. Liu, C.F. Greineder, E.R. Blankemeyer, R. Radhakrishnan, V. Muzykantov, Reduction of nanoparticle avidity enhances the selectivity of vascular targeting and PET detection of pulmonary inflammation, ACS Nano 7 (2013) 2461–2469.
[115] E.A. Simone, B.J. Zern, A.-M. Chacko, J.L. Mikitsh, E.R. Blankemeyer, S. Muro, R. V. Stan, V.R. Muzykantov, Endothelial targeting of polymeric nanoparticles stably labeled with the PET imaging radioisotope iodine-124, Biomaterials 33 (2012) 5406–5413.
[116] A. Abrimian, T. Kraft, Y.-X. Pan, Endogenous opioid peptides and alternatively spliced mu opioid receptor seven transmembrane carboxyl-terminal variants, Int. J. Mol. Sci. 22 (2021).
[117] J. Frigell, I. García, V. Gómez-Vallejo, J. Llop, S. Penadés, 68Ga-labeled gold glyconanoparticles for exploring blood-brain barrier permeability: preparation, biodistribution studies, and improved brain uptake via neuropeptide conjugation, J. Am. Chem. Soc. 136 (2014) 449–457.
[118] K. Siwowska, R.M. Schmid, S. Cohrs, R. Schibli, C. Müller, Folate receptor-positive gynecological cancer cells: In vitro and in vivo characterization, Pharmaceuticals (Basel, Switzerland) 10 (2017).
[119] J.T. Price, T. Tiganis, A. Agarwal, D. Djakiew, E.W. Thompson, Epidermal growth factor promotes MDA-MB-231 breast cancer cell migration through a phosphatidylinositol 3'-kinase and phospholipase C-dependent mechanism, Cancer Res. 59 (1999) 5475–5478.
[120] D. Takabatake, T. Fujita, T. Shien, K. Kawasaki, N. Taira, S. Yoshitomi, H. Takahashi, Y. Ishibe, Y. Ogasawara, H. Doihara, Tumor inhibitory effect of gefitinib (ZD1839, Iressa) and taxane combination therapy in EGFR-overexpressing breast cancer cell lines (MCF7/ADR, MDA-MB-231), Int. J. Cancer 120 (2007) 181–188.
[121] H. Wang, P. Guo, Radiolabeled RNA nanoparticles for highly specific targeting and efficient tumor accumulation with favorable in vivo biodistribution, Mol. Pharm. 18 (2021) 2924–2934.
[122] S. Ganesh, A.K. Iyer, D.V. Morrissey, M.M. Amiji, Hyaluronic acid based self-assembling nanosystems for CD44 target mediated siRNA delivery to solid tumors, Biomaterials 34 (2013) 3489–3502.
[123] B. Hu, Y. Ma, Y. Yang, L. Zhang, H. Han, J. Chen, CD44 promotes cell proliferation in non-small cell lung cancer, Oncol. Lett. 15 (2018) 5627–5633.
[124] M.B. Penno, J.T. August, S.B. Baylin, M. Mabry, R.I. Linnoila, V.S. Lee, D. Croteau, X.L. Yang, C. Rosada, Expression of CD44 in human lung tumors, Cancer Res. 54 (1994) 1381–1387.
[125] S. Ganesh, A.K. Iyer, F. Gattacceca, D.V. Morrissey, M.M. Amiji, In vivo biodistribution of siRNA and cisplatin administered using CD44-targeted hyaluronic acid nanoparticles, J. Control. Release 172 (2013) 699–706.
[126] W.J. Akers, Z. Zhang, M. Berezin, Y. Ye, A. Agee, K. Guo, R.W. Fuhrhop, S. A. Wickline, G.M. Lanza, S. Achilefu, Targeting of alpha(nu)beta(3)-integrins expressed on tumor tissue and neovasculature using fluorescent small molecules and nanoparticles, Nanomedicine (Lond.) 5 (2010) 715–726.
[127] S. Ganesh, A.K. Iyer, J. Weiler, D.V. Morrissey, M.M. Amiji, Combination of siRNA-directed gene silencing with cisplatin reverses drug resistance in human non-small cell lung cancer, Molecular Therapy. Nucleic Acids 2 (2013) e110.
[128] R.D. Klausner, G. Ashwell, J. van Renswoude, J.B. Harford, K.R. Bridges, Binding of apotransferrin to K562 cells: explanation of the transferrin cycle, PNAS 80 (1983) 2263–2266.
[129] M.D. Kleven, S. Jue, C.A. Enns, Transferrin receptors TfR1 and TfR2 bind transferrin through differing mechanisms, Biochemistry 57 (2018) 1552–1559.
[130] A.P. West, M.J. Bennett, V.M. Sellers, N.C. Andrews, C.A. Enns, P.J. Bjorkman, Comparison of the interactions of transferrin receptor and transferrin receptor 2 with transferrin and the hereditary hemochromatosis protein HFE, J. Biol. Chem. 275 (2000) 38135–38138.
[131] S.E. Lupold, B.J. Hicke, Y. Lin, D.S. Coffey, Identification and characterization of nuclease-stabilized RNA molecules that bind human prostate cancer cells via the prostate-specific membrane antigen, Cancer Res. 62 (2002) 4029–4033.
[132] B.S. Hendriks, S.G. Klinz, J.G. Reynolds, C.W. Espelin, D.F. Gaddy, T.J. Wickham, Impact of tumor HER2/ERBB2 expression level on HER2-targeted liposomal doxorubicin-mediated drug delivery: multiple low-affinity interactions lead to a threshold effect, Mol. Cancer Ther. 12 (2013) 1816–1828.
[133] D. Lakayan, R. Haselberg, R. Gahoual, G.W. Somsen, J. Kool, Affinity profiling of monoclonal antibody and antibody-drug-conjugate preparations by coupled liquid chromatography-surface plasmon resonance biosensing, Anal Bioanal Chem 410 (2018) 7837–7848.
[134] U.B. Nielsen, D.B. Kirpotin, E.M. Pickering, K. Hong, J.W. Park, M. Refaat Shalaby, Y. Shao, C.C. Benz, J.D. Marks, Therapeutic efficacy of anti-ErbB2 immunoliposomes targeted by a phage antibody selected for cellular endocytosis, BBA 1591 (2002) 109–118.
[135] M. Horikawa, Y. Shigeri, N. Yumoto, S. Yoshikawa, T. Nakajima, Y. Ohfune, Syntheses of potent leu-enkephalin analogs possessing beta-hydroxy-alpha, alpha-disubstituted-alpha-amino acid and their characterization to opioid receptors, Bioorg. Med. Chem. Lett. 8 (1998) 2027–2032.
[136] L. Terenius, A. Wahlström, G. Lindeberg, S. Karlsson, U. Ragnarsson, Opiate receptor affinity of peptides related to leu-enkephalin, Biochem. Biophys. Res. Commun. 71 (1976) 175–179.
[137] C.L. Esposito, D. Passaro, I. Longobardo, G. Condorelli, P. Marotta, A. Affuso, V. de Franciscis, L. Cerchia, A neutralizing RNA aptamer against EGFR causes selective apoptotic cell death, PLoS One 6 (2011) e24071.
[138] C. Chen, J. Ke, X.E. Zhou, W. Yi, J.S. Brunzelle, J. Li, E.-L. Yong, H.E. Xu, K. Melcher, Structural basis for molecular recognition of folic acid by folate receptors, Nature 500 (2013) 486–489.
[139] D. Bhattacharya, D. Svechkarev, J.J. Souchek, T.K. Hill, M.A. Taylor, A. Natarajan, A.M. Mohs, Impact of structurally modifying hyaluronic acid on CD44 interaction, J. Mater. Chem. B 5 (2017) 8183–8192.
[140] L.-K. Liu, B.C. Finzel, Fragment-based identification of an inducible binding site on cell surface receptor CD44 for the design of protein-carbohydrate interaction inhibitors, J. Med. Chem. 57 (2014) 2714–2725.
[141] W. Wang, Q. Wu, M. Pasuelo, J.S. McMurray, C. Li, Probing for integrin alpha v beta3 binding of RGD peptides using fluorescence polarization, Bioconjug. Chem. 16 (2005) 729–734.
[142] Y. Zheng, S. Ji, A. Czerwinski, F. Valenzuela, M. Pennington, S. Liu, FITC-conjugated cyclic RGD peptides as fluorescent probes for staining integrin αvβ3/αvβ5 in tumor tissues, Bioconjug. Chem. 25 (2014) 1925–1941.
[143] S. Ji, A. Czerwinski, Y. Zhou, G. Shao, F. Valenzuela, P. Sowiński, S. Chauhan, M. Pennington, S. Liu, (99m)Tc-galacto-RGD2: a novel 99mTc-labeled cyclic RGD peptide dimer useful for tumor imaging, Mol. Pharm. 10 (2013) 3304–3314.
[144] L. Wang, J. Shi, Y.-S. Kim, S. Zhai, B. Jia, H. Zhao, Z. Liu, F. Wang, X. Chen, S. Liu, Improving tumor-targeting capability and pharmacokinetics of (99m)Tc-labeled cyclic RGD dimers with PEG(4) linkers, Mol. Pharm. 6 (2009) 231–245.
[145] J. Shi, L. Wang, Y.-S. Kim, S. Zhai, Z. Liu, X. Chen, S. Liu, Improving tumor uptake and excretion kinetics of 99mTc-labeled cyclic arginine-glycine-aspartic (RGD) dimers with triglycine linkers, J. Med. Chem. 51 (2008) 7980–7990.
[146] M. Kumar, P. Kulkarni, S. Liu, N. Chemuturi, D.K. Shah, Nanoparticle biodistribution coefficients: a quantitative approach for understanding the tissue distribution of nanoparticles, Adv. Drug Deliv. Rev. 194 (2023) 114708.
[147] S. Wang, E.E. Dormidontova, Nanoparticle design optimization for enhanced targeting: Monte Carlo simulations, Biomacromolecules 11 (2010) 1785–1795.
[148] M.R. Caplan, E.V. Rosca, Targeting drugs to combinations of receptors: a modeling analysis of potential specificity, Ann. Biomed. Eng. 33 (2005) 1113–1124.
[149] N.A. Licata, A.V. Tkachenko, Kinetic limitations of cooperativity-based drug delivery systems, Phys. Rev. Lett. 100 (2008) 158102.
[150] A. Quintana, E. Raczka, L. Piehler, I. Lee, A. Myc, I. Majoros, A.K. Patri, T. Thomas, J. Mulé, J.R. Baker, Design and function of a dendrimer-based therapeutic nanodevice targeted to tumor cells through the folate receptor, Pharm. Res. 19 (2002) 1310–1316.
[151] F. Danhier, B. Vroman, N. Lecouturier, N. Crokart, V. Pourcelle, H. Freichels, C. Jérôme, J. Marchand-Brynaert, O. Feron, V. Préat, Targeting of tumor endothelium by RGD-grafted PLGA-nanoparticles loaded with paclitaxel, J. Control. Release 140 (2009) 166–173.
[152] C.B. Carlson, P. Mowery, R.M. Owen, E.C. Dykhuizen, L.L. Kiessling, Selective tumor cell targeting using low-affinity, multivalent interactions, ACS Chem. Biol. 2 (2007) 119–127.

[153] A. Myc, A.K. Patri, J.R. Baker, Dendrimer-based BH3 conjugate that targets human carcinoma cells, Biomacromolecules 8 (2007) 2986–2989.
[154] J. Huskens, Models and methods in multivalent systems, in: J. Huskens, L.J. Prins, R. Haag, B.J. Ravoo (Eds.), Multivalency, Wiley, 2018, pp. 23–74.
[155] G. Vauquelin, S.J. Charlton, Exploring avidity: understanding the potential gains in functional affinity and target residence time of bivalent and heterobivalent ligands, Br. J. Pharmacol. 168 (2013) 1771–1785.
[156] W.C.W. Chan, Principles of nanoparticle delivery to solid tumors, BME Front 4 (2023).
[157] A.S. Drozdov, P.I. Nikitin, J.M. Rozenberg, Systematic review of cancer targeting by nanoparticles revealed a global association between accumulation in tumors and spleen, Int. J. Mol. Sci. 22 (2021).
[158] M.P. Monopoli, D. Walczyk, A. Campbell, G. Elia, I. Lynch, F.B. Bombelli, K. A. Dawson, Physical-chemical aspects of protein corona: relevance to in vitro and in vivo biological impacts of nanoparticles, J. Am. Chem. Soc. 133 (2011) 2525–2534.
[159] C.D. Walkey, J.B. Olsen, H. Guo, A. Emili, W.C.W. Chan, Nanoparticle size and surface chemistry determine serum protein adsorption and macrophage uptake, J. Am. Chem. Soc. 134 (2012) 2139–2147.
[160] Y. Huai, M.N. Hossen, S. Wilhelm, R. Bhattacharya, P. Mukherjee, Nanoparticle interactions with the tumor microenvironment, Bioconjug. Chem. 30 (2019) 2247–2263.
[161] Z.P. Lin, L.N.M. Nguyen, B. Ouyang, P. MacMillan, J. Ngai, B.R. Kingston, S. M. Mladjenovic, W.C.W. Chan, Macrophages actively transport nanoparticles in tumors after extravasation, ACS Nano 16 (2022) 6080–6092.
[162] M.A. Miller, R. Chandra, M.F. Cuccarese, C. Pfirschke, C. Engblom, S. Stapleton, U. Adhikary, R.H. Kohler, J.F. Mohan, M.J. Pittet, R. Weissleder, Radiation therapy primes tumors for nanotherapeutic delivery via macrophage-mediated vascular bursts, Sci. Transl. Med. 9 (2017).
[163] M.A. Miller, Y.-R. Zheng, S. Gadde, C. Pfirschke, H. Zope, C. Engblom, R. H. Kohler, Y. Iwamoto, K.S. Yang, B. Askevold, N. Kolishetti, M. Pittet, S. J. Lippard, O.C. Farokhzad, R. Weissleder, Tumour-associated macrophages act as a slow-release reservoir of nano-therapeutic PT(IV) pro-drug, Nat. Commun. 6 (2015) 8692.
[164] Q. Dai, S. Wilhelm, D. Ding, A.M. Syed, S. Sindhwani, Y. Zhang, Y.Y. Chen, P. MacMillan, W.C.W. Chan, Quantifying the ligand-coated nanoparticle delivery to cancer cells in solid tumors, ACS Nano 12 (2018) 8423–8435.
[165] D. Kovács, N. Igaz, A. Marton, A. Rónavári, P. Bélteky, L. Bodai, G. Spengler, L. Tiszlavicz, Z. Rázga, P. Hegyi, C. Vizler, I.M. Boros, Z. Kónya, M. Kiricsi, Core-shell nanoparticles suppress metastasis and modify the tumour-supportive activity of cancer-associated fibroblasts, J. Nanobiotechnol. 18 (2020) 18.
[166] O. Zimmer, M. Walter, M. Remmert, O. Maier, R. Witzgall, A. Goepferich, Impact of interferon-γ on the target cell tropism of nanoparticles, J. Control. Release 362 (2023) 325–341.
[167] S. Maslanka Figueroa, D. Fleischmann, S. Beck, P. Tauber, R. Witzgall, F. Schweda, A. Goepferich, Nanoparticles mimicking viral cell recognition strategies are superior transporters into mesangial cells, Advanced Science 7 (11) (2020) 1903204.
[168] D. Fleischmann, S. Maslanka Figueroa, S. Beck, K. Abstiens, R. Witzgall, F. Schweda, P. Tauber, A. Goepferich, Adenovirus-Mimetic Nanoparticles: Sequential Ligand-Receptor Interplay as a Universal Tool for Enhanced in Vitro/In Vivo Cell Identification, ACS Applied Materials & Interfaces 12 (2020) 34689–34702.
[169] M. Bohley, A.E. Dillinger, F. Schweda, A. Ohlmann, B.M. Braunger, E.R. Tamm, A. Goepferich, A single intravenous injection of cyclosporin A-loaded lipid nanocapsules prevents retinopathy of prematurity, Science Advances 8 (2022) eabo6638.
[170] M. Bohley, A.E. Dillinger, B.M. Braunger, E.R. Tamm, A. Goepferich, Intravenous injection of cyclosporin A loaded lipid nanocapsules fights inflammation and immune system activation in a mouse model of diabetic retinopathy, Drug Delivery and Translational Research (2023) 1–12.
[171] D. Peterhoff, S. Thalhauser, J.M. Sobczak, M.O. Mohsen, C. Voigt, N. Seifert, P. Neckermann, A. Hauser, S. Ding, Q. Sattentau, M.F. Bachmann, M. Breunig, R. Wagner, Augmenting the immune response against a stabilized HIV-1 clade C envelope trimer by silica nanoparticle delivery, Vaccines 9 (2021).
[172] L. van der Zee, A. Corzo Remigio, L.W. Casey, I. Purwadi, J. Yamjabok, A. van der Ent, G. Kootstra, M.G.M. Aarts, Quantification of spatial metal accumulation patterns in Noccaea caerulescens by X-ray fluorescence image processing for genetic studies, Plant Methods 17 (2021) 86.
[173] H.A. Miller, A.W. Magsam, A.W. Tarudji, S. Romanova, L. Weber, C.C. Gee, G. L. Madsen, T.K. Bronich, F.M. Kievit, Evaluating differential nanoparticle accumulation and retention kinetics in a mouse model of traumatic brain injury via ktrans mapping with MRI, Sci. Rep. 9 (2019) 16099.